Modeling of microplastics sedimentation

Specialization project 2025

3rd semester project of Master
in Mathematical Bioscience

December 19, 2025

Authors:
Rasmus W. Christiansen (71979)
Sif E. Christensen (82429)

Supervisor:
Jesper Schimdt

Roskilde University

Summary

In this project a model with two types of microplastic particles describing the dispersion of microplastics in water and sediment has been posed. The employed equation are of reaction-advection-diffusion type equations. The distinction between the two particles rely on the one being neutrally buoyant, particle A, and the other being negatively buoyant, particle B. a and b in non-dimensionalized form.

The transition from water to sediment was modeled purely by using functional expressions of the advection, representing the change in velocity once the microplastic meets the sediment layer. After transforming the equations into dimensionless forms, a Pechlét function in b (dimensionless form) appeared. The Pechlét function is the control of the bulk of the dynamics for the particle b.

Steady state solutions were obtained for both particle a and b. Numerical simulations show that particle a quickly goes to steady state and it was determined to simply utilize the steady state solution of a as an input to b, both while numerically simulating the system but also while solving for a steady state.

Steady state solutions were obtained by solving directly, yielding an implicit solution and by assuming a solution of power series form. Diffusion and the dirichlet boundary condition for the power series solution were perturbed, which yielded either similar solutions, or completely new solutions, respectively. Solutions were compared to corresponding perturbed numerical simulations and did not match.

In doing so, the system is solved with two methods, and several perturbations done to see how the system reacts and the operator changes. Results shows the steady state distribution of B where, with chosen parameter values, the two layers are not modeled in a meaningful way. Plotting B's distribution for several iterations of different magnitudes of advection the layer differences are better seen in the distribution.

Numerical experiments showed that increasing the magnitude of advection significantly impacts the distribution of b in both the water column and the sediment column. The change is attributed to the choice of boundary condition.

As for deriving power series solutions for b, it turned out that the integral of the steady state of a over the entire domain is an integration constant of b in its implicit form, but also the value of the free parameter in the power series solution. This clearly shows that both the advection and reaction are determining factor for b.

Use of generative AI

In this project, we used the following AI tools; Chat GPT (https://chatgpt.com/), and Microsoft CoPilot (https://copilot.microsoft.com/). The AI models were used as search engines, debugging python code, checking derivations of solutions and get feedback during the ideation phase of the project. We chose to use these tools because we wanted to get more specific and curated hits on our searches, improve python code quality and accelerate debugging of code and finally validate our mathematical derivations. This output was revised and edited such that we take responsibility for the final product.

Acknowledgment

This project has been made after inspirational talks with Kristian Syberg and Claudia Lorenz. A big thanks to them for taking time out of their busy schedules to meet, talk and exchange ideas and knowledge on the subject of microplastics.

A great thanks is owed to Jepser Schmidt Hansen, for great teaching, inspiration and supervision. This project had truly never existed without his help and guidance and always great spirit.

Table of Contents

1 Introduction

Plastic materials was first introduced in the 1950s and has been widespread in all industries ever since. Plastic offers barrier properties, is a durable material and generally has low density, making it applicable in many contexts, from beauty products, conservation of food, agriculture, to electronics. However, the versatility of plastics also makes them persisting in the environment over long periods of time. Their recalcitrant nature is good for many purposes but also make littered plastics long-lasting. In the environment the plastic break down into smaller and smaller fragments as time passes, until it becomes microplastics (MPs). MPs are defined as plastic fragments with a diameter of 5 mm or smaller [Microplastics, 29].

A study has estimated that around 2.7 million tonnes of MPs was emitted to the environment only in 2020, and that the amount is expected to double by 2040. [24]. Even though MPs existence in the environment, are abundant and rapidly increasing, not much is known about the effect on humans and the environment. MPs travel through food chains, and end up in organisms including human beings. MPs have been observed in human feces, placentas and brains. Environmental effects of MPs have been shown to be; slowing down the growth of phytoplankton, degrading soil fertility and killing 100.000 marine animals and more than a million seabirds every year, among many suspected effects [33, 11, 10].

Because many plastics are neutrally or buoyant they are easily dispersed in aquatic environments. As a consequence of this and the high durability of plastics, they are found almost everywhere. MPs in aquatic environments can travel long distances from their source point and can therefore be found in very remote places [29]. Global distribution of MPs varies considerably but depend on the presence of metropolitan areas, local hydrodynamic effects, use of the maritime area etc.. Even though the distribution of MPs is fluctuating substantially, it has been established that rates of accumulation are generally higher in the northern hemisphere compared to the southern and that MPs are more abundant in the sediment in enclosed seas such as the Mediterranean. [13].

In 2023 it was estimated that between 75 to 199 million metric tons of plastics was present in the ocean. [Environmental litteracy council]. Of this, 3 to 11 million tonnes of plastics is estimated to be on the seabed, and 3 million tonnes on the surface. [35]. The remainder however is hard to estimate the placement of. Some will be suspended in the water column and some will have worked its way down into the sediment layers. Arguably most microplastics in the sediment will be small in size to easily penetrate the seabed. The "missing plastics" has become a topic of interest, both to estimate the fate of MPs, but also the impacts on humans, marine life, and to determine where to focus a potential clean up effort [12].

It has been shown that non-bouyant MP particles will exhibit similar transport as natural sediments, but that shape heavily determines whether an MP will behave as

natural sediment [1]. Therefore one would expect that non-buoyant MPs are situated in the sediment, which they are, but as it turns out penetrate deeper than expected. Sediment cores from freshwater lakes reveal that microplastics have penetrated sediment layers dated to pre-1950s. Particles at this depth has a dimension that is $< 500\mu m$. The authors who report the results from the sediment core also show that the shape of the particle is crucial in determining the mobility of the particle [7].

Modeling case and focus

This project will model the vertical transport of microplastics in homogeneous seawater and sediment using reaction-advection-diffusion (RAD) equations. The intent of employing RAD equations is to determine how MPs distribute vertically in seawater and sediment layers. The general RAD equations can be further adapted to different scenarios. Scenarios such as to examine different sea or sediment depths, sediment grain properties or adding fluid flow fields to simulate plastic transportation in both the lateral dimensions as well as the vertical dimension.

To anchor the project in a real-world context, the case of off-shore wind parks as point-source emitters of microplastics will be examined. Horns rev I, II, and III (Figure 1) west of Esbjerg in the south of Jutland in Denmark will be utilized to determine sediment material composition and size range. As well as seawater characteristics. The MPs that are emitted from the windmill parks ranges from $30\mu m$ to $60\mu m$ in size. The amount of emitted MP has been estimated to be approx. 500g due to maintenance and 75g due to erosion pr. blade pr. year [Claudia Lorenz].

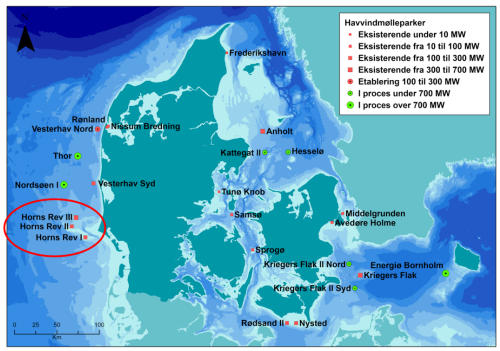

Figure 1: *Map of Denmark with existing offshore windparks with Horns rev I, II, and III highlighted in the red circle. The wind parks were established in 2002, 2009 and 2019 respectively. The map is taken from [8].*

Horns Rev (I, II, III) is situated in the North sea, close to the shore of Denmark, in the southern part of the North sea. Even though the southern part of the North sea is subjected to strong tidal and residual currents, stratification of the water column does occur during summer, although only at deep waters [5]. The parks are situated

at water depths between 0 and 15 meters depth where stratification is not expected to occur [25]. Therefore assuming a homogeneous water column when modeling is sensible.

The sediment in and around Horns Rev in 2005 has ranges in sizes between $347\mu m$ to $612\mu m$ and has an average median grain size of $494\mu m$ and does host bottom dwelling organisms [25]. Bottom-dwelling organisms actively mix the upper sediment layer through bioturbation, which effectively generates an advective flow within the sediment. Diffusion of MPs in the sediment, is expected to be occur, although small. Therefore both diffusion of advection will take place throughout the water and sediment column.

The above considerations leads to motivate the following research question that will guide the project;

> **How does a reaction-advection-diffusion model predict the distribution of microplastics the water column and sediment of the sea?**

2 Model formulation

Consider the vertical transport of microplastics (MP) in the marine environment. In this case both the water column and sediment will be included. Two particle types are considered, particle A and B. Particle A is neutrally buoyant and B negatively buoyant in seawater. Figure 2 illustrates the domain and the dynamics of the model in a conceptual diagram.

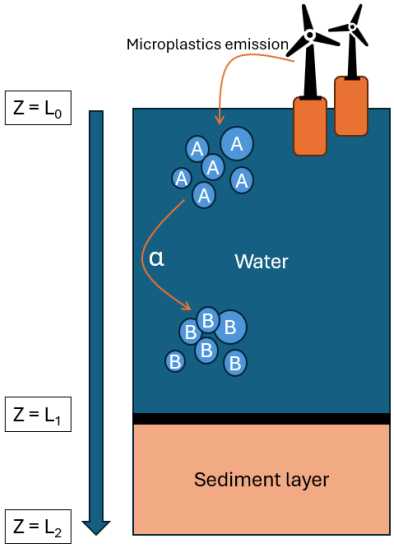

Figure 2: *Schematic of the single-compartment model for microplastic transport in 1 dimension. The compartment includes a water column and a sediment layer. Positions L_0, L_1, and L_2 correspond to the water surface, the seabed, and the system's lower boundary, respectively.*

Particle A will be transformed into B with a rate of α. This reaction occurs naturally by biofilm formation. Depending on the aggregating organism the density and size of the particle will increase [2]. Another contributor to changes in density of MP is fish accidentally ingesting MP's. This will encapsulate the MP into excreted feces and these will eventually settle on the seabed [18, 30].

The water and sediment is assumed to have no currents driving the advective transport and therefore only relative density differences between particle and water will contribute to advection. Particles will not be modeled as individual independent particles, but rather as a concentration moving through the water and sediment. This means that shape characteristics wont be taken into consideration, which has been reported as important for how a given particle distributes in the environment [7, 1]. In Figure 2 the blue arrow indicate the direction of the coordinate system, with 0 at

the sea surface and L_2 at end of the system. Note that L_2 is positive which in turn means that advection must be positive from 0 to L_2. Even though ocean currents dominate the transport of MP it is still relevant to model the distribution without a fluid flow [17]. By doing so, it isolates the inherent transport mechanism that operate independently of large scale circulation. Understanding the baseline dynamics provides a foundation for interpreting how MPs distribute by physical and biological processes. Once this has been done the addition of flow fields can be incorporated to capture combined effects.

Using the above, the focus is how particles A and B move through time and space with diffusion, advection and reaction processes. For this purpose consider the fluxes of A and B, in a given confined volume between z_1 and z_2, denoted Δz (figure 3).

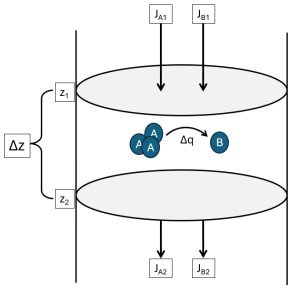

Figure 3: *Fluxes describing the rate of change of each of the particles A and B. Δz denotes the distance between z_1 and z_2. J_{A1} and J_{A2} are fluxes of A in and out of the compartment, and J_{B1} and J_{B2} for B. Δq is the conversion from A to B. Conversion rate is not 3A to 1B, the figure is meant as a conceptual drawing.*

The rate of change of the total concentrations of A and B (A_{tot} and B_{tot}) is given by fluxes at z_1 and z_2. The fluxes will be denoted and J_{A1}, J_{A2}, J_{B1} and J_{B2}. Let the general conversion rate from A to B be Δq. Then

$$\begin{aligned} \frac{dA_{tot}}{dt} &= J_{A1} - J_{A2} - \Delta q A_{tot} \\ \frac{dB_{tot}}{dt} &= J_{B1} - J_{B2} + \Delta q A_{tot} \end{aligned} \tag{1}$$

The above can be related to the actual concentration of A and B as such

$$\begin{aligned} A_{tot}(t) &= C_{area}\Delta z A(t), \\ B_{tot}(t) &= C_{area}\Delta z B(t) \end{aligned} \tag{2}$$

where $C_{area}\Delta z$ is the volume between z_1 and z_2. Taking the derivative of equation 2 yields

$$\begin{aligned} \frac{dA_{tot}}{dt} &= C_{area}\Delta z\frac{dA}{dt} \text{ and} \\ \frac{dB_{tot}}{dt} &= C_{area}\Delta z\frac{dB}{dt}. \end{aligned} \tag{3}$$

Now the derivative of the concentration with respects to time of A and B can be isolated as such

$$\begin{aligned} \frac{dA}{dt} &= -\frac{\Delta q A_{tot}}{C_{area}\Delta z} - \frac{1}{C_{area}}\frac{J_{A2}-J_{A1}}{\Delta z} \text{ and} \\ \frac{dB}{dt} &= \frac{\Delta q A_{tot}}{C_{area}\Delta z} - \frac{1}{C_{area}}\frac{J_{B2}-J_{B1}}{\Delta z}. \end{aligned} \tag{4}$$

The above equations in 4 must hold for any infinitesimally small volume and will therefore in the limit as $\Delta z \to 0$ depend on z and become:

$$\begin{aligned} \frac{\partial}{\partial t}A(t,z) &= -w(t,z) - \frac{\partial}{\partial z}J_A(t,z) \text{ and} \\ \frac{\partial}{dt}B(t,z) &= w(t,z) - \frac{\partial}{\partial z}J_B(t,z). \end{aligned} \tag{5}$$

J_A and J_B denote the net fluxes pr. unit volume, and w the conversion rate of particle A to B. w depends only on A and can be rewritten as $w(t,z) = r(A(t,z)) = \alpha A$. The magnitude of the fluxes J_A and J_B are sums of advection and diffusion. Each of the fluxes will have a natural removal of concentration due to diffusion, but only particle B will experience advection. Using Ficks law and the inherent advection of the particles the fluxes J_A and J_B are equated as such

$$\begin{aligned} J_A &= -D_A\frac{dA}{dz} \text{ and} \\ J_B &= -\left(D_B\frac{dB}{dz} + UB\right). \end{aligned} \tag{6}$$

Where U is a position dependent advection function, D_a and D_b diffusion constants for A and B, respectively. Substituting the above equations and $w = \alpha A$ into eqs. 5 yields the governing equations determining the vertical transport of particle A and B. The equations are

$$\frac{\partial A}{\partial t} = D_A\frac{\partial^2 A}{\partial z^2} - \alpha A \tag{7}$$

$$\frac{\partial B}{\partial t} = \frac{\partial}{\partial z}\left(D_B\frac{\partial B}{\partial z} + U(z)B\right) + \alpha A \tag{8}$$

Note that in the above U depend on z. Generally advection can depend position. The main reason for letting U depend on z is the nature of the compartment (figure 2). Other research in the field, have modeled the vertical transport of MP's alike this but in several compartments. However, we aim to create a model consisting of a single set

of equations, defining all of the domain. This is done by making advection parameters position dependent, thus changing the dynamics of the solution over the entirety of the domain.

The particles reside in an environment with two different media, namely seawater and sediment. Seawater and sediment have different properties, and will therefore influence transportation of the particles differently. Particles in sediment will travel at a different rate than in water. This influence will be accounted for by having advection, $U(z)$, as a function of position (eq.8). Diffusion of B can also be modeled to differ throughout the water column, but for the sake of simplicity it will be held constant. This is based on an assumption that the vertical transport is dominated by advection. Note that diffusion of particle A is constant and does not depend on position. The reason for this is that A is assumed to be neutrally buoyant. Diffusion occur over a long time scale, and A is assumed to never reach the sediment before being converted into B.

Advection of particle B is due only to relative differences in density between the particle and seawater. Advection of particles in sediment is especially relevant since a lot of bottom dwelling organisms rework the sediment. But as particles travel into the deeper sediment layers with very little or no oxygen the impact of biological activity is near zero [32, 20].

It has been shown through experiments that MPs of sizes around 1μm diffuse within the hyporheic zone (experiment done in the interface between groundwater and the riverbed) [6]. Although the MP particle size considered in this project is larger (30-60μm), diffusion within the sediment layer is still assumed to be valid.

2.1 Non-dimensionalization

The system introduced in equations 7 and 8 can be non-dimensionalized to eliminate units. To achieve this, characteristic length, time, concentrations and velocity should be introduced. There are two advantages of performing this transformation, one is that key parameters can be identified, and it removes the dependency on units, simplifying analysis. Now, by introducing the following dimensionless variables,

$$\begin{aligned} \tau = \frac{t}{T}, \gamma = \frac{z}{L} a = \frac{A}{A_0}, \\ b = \frac{B}{B_0}, u = \frac{U}{U_0}, d_b = \frac{D_B}{D_{B0}} \end{aligned} \tag{9}$$

and substituting into equations 7 and 8, dimensionless forms can be derived. Note that u is a spatial dependent function of γ, as advection forces will change when crossing from water to sediment. The equations come out as,

$$\begin{aligned}
\frac{1}{T}\frac{\partial(aA_0)}{\partial\tau} &= D_A\frac{\partial^2(aA_0)}{\partial\gamma^2} - \alpha a A_0, \\
\frac{1}{T}\frac{\partial(bB_0)}{\partial\tau} &= \frac{D_{B0}}{L^2}d_b\frac{\partial^2(bB_0)}{\partial\gamma^2} + \frac{U_0}{L}\left(u\frac{\partial(bB_0)}{\partial\gamma} + \frac{\partial u}{\partial\gamma}bB_0\right) + \alpha a(\tau,\gamma)A_0.
\end{aligned} \tag{10}$$

By letting the characteristic time, $T = L^2/D_A$ and $B_0 = A_0$ the equations above can be reduced substantially, as

$$\frac{\partial a}{\partial\tau} = \frac{\partial^2 a}{\partial\gamma^2} - \theta a \tag{11}$$

$$\frac{\partial b}{\partial\tau} = Dd_b\frac{\partial^2 b}{\partial\gamma^2} + Pe_a(\gamma)\left(u\frac{\partial b}{\partial\gamma} + \frac{\partial u}{\partial\gamma}b\right) + \theta a(\tau,\gamma). \tag{12}$$

where

$$Pe_a = \frac{U_0 L}{D_a}, \theta = T\alpha, D = \frac{D_{B0}}{D_A}, \tag{13}$$

The diffusion coefficient for particle A vanishes once the equations are non-dimensionalized. Still 11 and 12 have gained two parameters Pe_a and D, but by constructing new functions $\widehat{Pe_a}$ and $\hat{d}_b$ the system can be simplified even further. Let

$$\begin{aligned}
\widehat{Pe_a}(\gamma) &= Pe_a \cdot u(\gamma) \\
\hat{d}_b &= D \cdot d_b = \frac{D_{B0}}{D_A}\frac{D_B}{D_{B0}} = \frac{D_B}{D_A},
\end{aligned} \tag{14}$$

then the equations 11 and 12 simplify to

$$\frac{\partial a}{\partial\tau} = \frac{\partial^2 a(\tau,\gamma)}{\partial\gamma^2} - \theta a(\tau,\gamma), \tag{15}$$

$$\frac{\partial b(\tau,\gamma)}{\partial\tau} = \frac{\partial}{\partial\gamma}\left(\hat{d}_b\frac{\partial b(\tau,\gamma)}{\partial\gamma} + \widehat{Pe_a}(\gamma)b(\tau,\gamma)\right) + \theta a(\tau,\gamma). \tag{16}$$

The above equations are non-dimensional forms of the formulated system.

2.2 Advection of B

As mentioned, advection of particle b will be modeled as a function of position. This is effectively the so called Pechlét function, $\widehat{Pe_a}$ that becomes position dependent. The Pechlét function is a measure of the relation between the advection and the diffusion. Since diffusion here is position independent, the advection will be controlling the spatial dependency of the Pechlét function. $\widehat{Pe_a}$, will be assumed to be stable throughout the water column, but exhibits a sharp change near L_1 (figure 2). From literature it is shown that water stratification has no impact on vertical distribution of microplastics in the area, thus density changes in the water column can be disregarded [14]. Between L_1 and L_2 the magnitude of parameters will decrease as well, modeling the transition

between water and sediment. The functional expression for $\widehat{Pe_a}$ must be chosen carefully. In order to ease the analysis and derivation of steady states polynomials are used.
There are two main advantages of using polynomials. Polynomials are smooth, and they will be easier to manipulate whenever analytical expressions are to be obtained. For the sake of this project, advection in the water column will be modeled as the terminal settling velocity of the B. Using Stokes' Law of settling, the terminal velocity of particle B can be estimated [19]. Knowing that most coating from windmill is made from epoxy resin and polyurethane with densities between 1.0 to 1.3 g/cm^3, and that biofilm formation increase the density of MPs anywhere between 10% and 40% the settling velocity can be estimated [Claudia Lorenz, 26]. Furthermore, non pristine and negatively buoyant MPs in the size range 0.02mm to 4.92mm, have settling velocities that are up to 130% slower compared to similar particles where biofilm has formed [22].
Assuming that the mean density of the particle will increase 20% due to biofilm formation, settling velocity in the water column is estimated to be $6.02 \cdot 10^{-4} m/s$.
The sediment will act as a barrier, and if not for bioturbation the advective term would be close to zero. The expectation is that bioturbation pr. unit area will be 10 times slower than in the water column.

Advection will be modeled by a 4th degree polynomial which has been fitted to a sigmoidal function. The sigmoidal function has two plateaus, one for the estimated velocity in the water column and the other for velocity in the sediment. Look to Figure 4 for a representation of the advection. Note that variables in Figure 4 are non-dimensional.

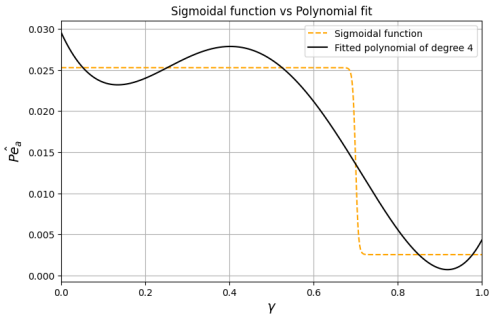

Figure 4: *Orange dotted curve is a sigmoidal function where each plateau represent the settling velocity in the water column and in sediment, from left to right. The black curve is a fitted fourth degree polynomial. In the domain* $\gamma \in [0, 1]$ *the fitted polynomial attain no negative values. Coefficients of polynomial are, with highest degree first,* $0.563, -1.092, 0.616, -0.111, 0.030$.

The curve in Figure 4 is given by

$$\widehat{Pe_a}(\gamma) = 0.03 - 0.111\gamma + 0.616\gamma^2 - 1.092\gamma^3 + 0.563\gamma^4. \tag{17}$$

For the sake of this project $\widehat{Pe_a}(\gamma)$ must be positive in the domain $\gamma \in [0, 1]$. From Figure 4 the expression never becomes 0 for $\gamma \in [0, 1]$.

2.3 Boundary and Initial Conditions

The boundary and initial conditions to equation 15 are set up as following:
The non-dimensionalized concentration of particles of type A is modeled with Dirichlet boundary conditions:

$$\begin{aligned} a(\tau, 0) &= 1 \\ a(\tau, 1) &= 0 \end{aligned} \tag{18}$$

This assumes a unity surface concentration, thus will be able to give a relative measure of the concentration. The zero boundary at the bottom of the system assumes all particles have been transformed into type B particles before reaching position $\gamma = 1$, corresponding to $z = L_2$ in the dimensional system. An initial condition adhering to these have been chosen to be

$$a(0, \gamma) = \frac{e^{-g\gamma} - e^{-g}}{1 - e^{-g}} \tag{19}$$

This gives an exponential function that adheres to the boundary conditions, g determines how steeply it decreases towards 0.
The concentration of particles of type B are modeled by the boundary conditions:

$$\begin{aligned} b(\tau, 0) &= 0 \\ J_b(\tau, 1) &= 0 \end{aligned} \tag{20}$$

where J_b determines the flux of the system defined by

$$J_b(\tau, \gamma) = -\hat{d}_b \frac{\partial b}{\partial \gamma}(\tau, \gamma) - \widehat{Pe}_a(\gamma)\, b(\tau, \gamma). \tag{21}$$

.
The initial condition:

$$b(0, \gamma) = 0 \tag{22}$$

will hold both boundary conditions since no flux can exist when the concentration is zero.
This assumes no B particles exist when instantiation of the system begins, and B will only exist from A particles being transformed into B.
The null-flux boundary at the bottom of the system, is a Robin Boundary condition, since it in a diffusion-advection system will be a linear combination of Neumann and Dirichlet boundary conditions:

$$J_b(\tau, \gamma) = D_B(\gamma) \frac{\partial b}{\partial \gamma} + U(\gamma) b(\gamma) \tag{23}$$

Thus the diffusion and advection will have to balance at this boundary, so non of the particles can leave the domain at this boundary. This models an impermeable boundary, which in our case will model a layer beneath the sediment impenetrable by the microplastics. This is a far-field approximation, since we assume we are far enough down into the sediment to reach a impermeable layer, like a rock surface.

2.4 Full model

Governing equations:

$$\frac{\partial a}{\partial \tau}(\tau,\gamma) = \frac{\partial^2 a}{\partial \gamma^2}(\tau,\gamma) - \theta\, a(\tau,\gamma), \tag{24}$$

$$\frac{\partial b}{\partial \tau}(\tau,\gamma) = \frac{\partial}{\partial \gamma}\left(\hat{d}_b \frac{\partial b}{\partial \gamma}(\tau,\gamma) + \widehat{Pe}_a(\gamma)\, b(\tau,\gamma)\right) + \theta\, a(\tau,\gamma). \tag{25}$$

Boundary conditions:

$$\begin{aligned} a(\tau,0) &= 1, \qquad & a(\tau,1) &= 0, \\ b(\tau,0) &= 0, \qquad & J_b(\tau,1) &= 0, \end{aligned} \tag{26}$$

where the flux J_b is defined as

$$J_b(\tau,\gamma) = -\hat{d}_b \frac{\partial b}{\partial \gamma}(\tau,\gamma) - \widehat{Pe}_a(\gamma)\, b(\tau,\gamma). \tag{27}$$

Initial conditions:

$$a(0,\gamma) = \frac{e^{-g\gamma} - e^{-g}}{1 - e^{-g}}, \qquad b(0,\gamma) = 0. \tag{28}$$

2.5 Parameters

Parameter	**Quantitative description**	**Qualitative description**
A, B	$A(t,z)$, $B(t,z)$	State variables describing the concentration of neutrally and negatively bouyant particles A and B.
D_A	Na	Diffusion coefficient for diffusion of A.
D_B	Na	Diffusion coefficient for diffusion of B.
α	Na	Reaction rate from A to B.
$U(z)$	4th order degree polynomial	Position depending advection coefficient. The function describes the magnitude of the advective coefficient.
τ	$\tau = t/T$	Non-dimensional time.
γ	$\gamma = z/L$	Non-dimensional length. L is the characteristic length.
$a(\tau,\gamma)$	$a = A/A_0$	Non-dimensional concentration of A. A_0 is a characteristic concentration in A.
$b(\tau,\gamma)$	$b = B/B_0$	Non-dimensional concentration of B. B is a characteristic concentration in B.
$u(\gamma)$	$u = U/U_0$	Non-dimensional advective parameter. U_0 is a characteristic advection.
d_b	$d_b = D_B/D_A$	Dimensionless diffusion.
T	$T = L^2/D_A$	Characteristic time.
θ	$\theta = T\alpha$	Non-dimensional reaction rate from a to b.
$Pe_a(\gamma)$	$Pe_a(\gamma) = U_0 L/D_a$	Pechlét function. Fraction between amount of advection and diffusion.
$\widehat{Pe_a(\gamma)}$	$\widehat{Pe_a(\gamma)} = Pe_a u(\gamma)$	Position depend Pechlét function.
L_0, L_1, L_2	Na	Sea surface, sea floor, total length of simulated domain. L_2 can also be thought of as an impermeable sediment layer.
$J_b(\tau,\gamma)$	$J_b(\tau,\gamma) = \hat{d_b}\partial b/\partial\gamma + \hat{Pe_a}(\gamma)b$	Flux in b.

3 Theory

The system as defined in section 2.4 will in the following sections be analyzed. Analytical expressions for steady states will be derived and properties of the derived equations will be highlighted. In order to properly state anything about the results relevant mathematical theory must be stated.

3.1 Power series method

For the general differential equation of power n:

$$a_0(x)\frac{d^n c}{dx^n} + a_1(x)\frac{d^{n-1}c}{dx^{n-1}} + ...a_n(x)y = 0, \tag{29}$$

with $2 \leq n$ and x defined in a given domain from $[b_1, b_2]$ and $n \in \mathbb{N}$. If the varying coefficients are polynomials or other smooth and differentiable functions, one can often find solutions to equation 29 of the form

$$y(x) = \sum_{n=0}^{\infty} c_n y^n. \tag{30}$$

Equation 30 is then differentiated the appropriate amount of times and substituted into the 29. Differentiating equation 30 can be generalized as

$$\frac{d^{(k)}y}{dx^{(k)}} = \sum_{n=k}^{\infty} c_n n(n-1)...(n-k+1)x^{n-k}, \tag{31}$$

for $x \in]-\rho, \rho[$ where ρ is the radius of convergence and $k \in \mathbb{N}$ is the order of the ODE. After substituting into the original equation (29), then everything is collected as

$$\sum_{n=0}^{\infty} b_n x^n = 0. \tag{32}$$

Where b_n represents the product of coefficients from the original (equation 29) and coefficients from the differentiation process in equation 31. A very useful result of power series is that the series are guaranteed to converge for a given interval of x values. This leads to the following theorem

Theorem 1 *For any power series of the form $\sum_{n=0}^{\infty} c_n x^n$ one of the following holds:*

- *The series is convergent for $x = 0$.*
- *The series is absolutely convergent for all $x \in \mathbb{R}$.*
- *There exists a number $\rho > 0$ such that the series is absolutely convergent for $\rho > |x|$ and divergent for $|x| > \rho$.*

The proof of theorem 1 above can be found in [3] appendix A.8.

After getting the entire ODE on the form of equation 32 it follows that for all n that $b_n = 0$, since

$$\begin{aligned} &n = 0 : b_0 = 0 \\ &n = 1 : 0 + b_1 x = 0 \implies b_1 = 0 \\ &n = 2 : 0 + 0 + b_2 x^2 = 0 \implies b_2 = 0 \\ &\quad \cdots \\ &n = n : 0 + 0 + ... + b_n x^n = 0 \implies b_n = 0. \end{aligned} \tag{33}$$

dette er forkert

This leads to the determination of the coefficients c_n since b_n is a product of coefficients from equations 29 and 31. One then proceeds to express the coefficients b_n in terms of c_n. The coefficients c_n for the purpose of this project will be given as the coefficients of a polynoimal of order m [3].

3.2 Sturm–Liouville theory

Given equations of the general form

$$c_2(x)\frac{d^2y}{dx^2} + c_1(x)\frac{dy}{dx} + c_0(x)y = f(x), \tag{34}$$

The Sturm-Liouville form can be computed by introducing an integrating factor and collecting terms as such

$$F(x) = \frac{d}{dx}\left(p(x)\frac{dy}{dx}\right) + q(x)y.$$

Where

$$\begin{aligned} p(x) &= e^{\int \frac{c_1}{c_2} dx}, \\ q(x) &= p(x)\frac{c_0(x)}{c_2(x)}, \text{ and} \\ F(x) &= p(x)\frac{f(x)}{c_2(x)} \end{aligned} \tag{35}$$

yields the Sturm Liouville form. This is well-defined as long as $c_2 \neq 0 \forall x \in I$, where I is the domain of the system.
Utilizing the above, the Sturm-Liouville operator is defined as

$$\mathcal{L} = \frac{d}{dx}p(x)\frac{d}{dx} + q(x). \tag{36}$$

The problem in 35 can be written as an eigenvalue problem as:

$$-(p(x)b')' + q(x)b = \lambda w(x)b. \tag{37}$$

b=y?

and using operator notation equations 35 and 37

$$\begin{aligned} \mathcal{L}y &= f, \\ \mathcal{L}\phi_n &= -\lambda_n \sigma(x)\phi_n. \end{aligned} \tag{38}$$

Where $y(x)$ is assumed to be a sum of eigenfunctions, such that

$$y(x) = \sum_{n=1}^{\infty} c_n \phi_n(x). \tag{39}$$

ϕ_n is an eigenfunction, λ_n is its corresponding eigenvalue and, $\sigma(x)$ a weight function. There are several useful properties of regular Sturm-Liouville problems, but only one property is relevant for this project. An important property of Sturm-Liouville problems is that

- Eigenvalues are real, countable, ordered and there is a smallest eigenvalue. I.e. $\lambda_1 < \lambda_2 < ... < \lambda_n$, but there is no largest eigenvalue and $n \to \infty$ then $\lambda_n \to \infty$.

A problem is regular whenever the coefficients of 37 are continuous and larger than 0. Specifically it is required that $p(x)$, $p'(x)$, $q(x)$ and $\sigma(x)$ are continuous functions, and that $p(x) > 0$, $\sigma(x) > 0$. All requirements must be satisfied on the given interval I. Furthermore, Sturm-Liouville operators are self-adjoint and the following must hold:

$$\begin{aligned} &1)\ \langle u, \mathcal{L}[v] \rangle = \langle \mathcal{L}[u], v \rangle \\ &2)\ p(x) > 0, q(x) \in \Re \end{aligned} \tag{40}$$

for all u, v's satisfying the boundary conditions [31].
The inner product is defined by

$$\langle u, v \rangle = \int_a^b u^*(x) v(x) dx, \tag{41}$$

where $[a, b]$ is the interval of the domain and $*$ denotes the complex conjugate of u.
Lastly the second Fredholm Alternative will be defined. The alternative is useful whenever dealing with problems where the homogenous part of the solution is the trivial solution because it guarantees uniqueness [16].

Theorem 2 *A solution of $Ax = b$, if it exists, is unique iff $x = 0$ is the only solution of $Ax = 0$.*

The proof of the theorem can be found in [16].

3.3 Numerical and computational methods

All numerical simulations of the equations in 16 will be performed using an altered FTCS (forward time-centered space) algorithm. The alteration consist of computing the advection term using an upwind finite difference.

For the sake of describing the employed method let c be a dynamic variable. The evolution of c through time and space is described as

$$\frac{\partial b}{\partial t} = D\frac{\partial^2 c}{\partial x^2} + U\frac{\partial c}{\partial x} + Rc. \tag{42}$$

In above D, U, and R are diffusion, advection, and reaction constants. Let D, U, and $R < 0$ Now, to discretize time and space let i and n denote the discretized space and time point, and Δx and Δt the size of step in space and time respectively. Then the second and first order in space and first order in time will be approximated as:

over ik under

$$\begin{aligned}
\frac{\partial^2 c}{\partial x^2} &= \frac{c_{i-1}^n - 2c_i^n + c_{i+1}^n}{\Delta x^2} + \mathcal{O}(\Delta x^2) \\
\frac{\partial c}{\partial x} &= \frac{c_i^n - c_{i-1}^n}{\Delta x} + \mathcal{O}(\Delta x^2) \\
\frac{\partial c}{\partial t} &= \frac{c_i^{n+1} - c_i^n}{\Delta t} + \mathcal{O}(\Delta t)
\end{aligned} \tag{43}$$

By using the approximate forms of the derivatives in space, time and omitting the error terms the above can be inserted into equation 42. After inserting, c_i^{n+1} can be isolated as such:

$$c_i^{n+1} = c_i^n + \Delta t\left(D\frac{c_{i-1}^n - 2c_i^n + c_{i+1}^n}{\Delta x^2} + U\frac{c_i^n - c_{i-1}^n}{\Delta x} + Rc_i^n\right). \tag{44}$$

For all performed simulations only null-flux and Dirichlet boundary conditions are employed. The Dirichlet will be approached by forcing the boundary point to be 0. Let 1 be the smallest and q be the largest index on discretized domain, then

$$c_1^n = 0 \text{ or } c_q^n = 0. \tag{45}$$

And for the null-flux boundary condition for the smallest index it will be a forwards difference

$$\begin{aligned}
0 &= D\frac{c_1^n - c_2^n}{\Delta x} + Uc_1^n, \\
c_1^n &= \frac{c_2^n \frac{D}{\Delta x}}{U + \frac{D}{\Delta x}}.
\end{aligned} \tag{46}$$

And for the largest index in the domain the backwards difference will be employed as

$$\begin{aligned}
0 &= D\frac{c_q^n - c_{q-1}^n}{\Delta x} + Uc_q^n, \\
c_q^n &= \frac{c_{q-1}^n \frac{D}{\Delta x}}{U + \frac{D}{\Delta x}}.
\end{aligned} \tag{47}$$

To ensure stability of the FCTS algorithm the Neumann stability criterion has been used, alongside the CFL criterion when choosing the step forwards in time [27, 28].

The Neumann criterion is in the case of this model is $\Delta t < \Delta x^2/2D$ and the CFL criterion as $\Delta t < \Delta x/|U|$. The step forwards in time should be smaller than both of the criteria such that

$$\Delta t < \min\left(\frac{\Delta x^2}{2D}, \frac{\Delta x}{|U|}\right). \tag{48}$$

Furthermore, ad hoc calculations, simplifications and graphical representations of expressions have been performed using the MapleSoft software **Maple** (https://www.maplesoft.com/products/Maple/).

All numerical simulations are performed using the `python` programming language. All the code related to this project can be found at the GitHub repository (https://github.com/rasmchr/Specialisation-project-RUC).

4 Steady state solution to a

As seen in equations 15 and 16 particle a is independent from b. Thus a solution to the concentration of a in steady state can be obtained. The equation to be examined is

$$\frac{\partial a}{\partial \tau} = \frac{\partial^2 a}{\partial \gamma^2} - \theta a \tag{49}$$

with initial condition

$$a(\gamma, 0) = \tfrac{e^{-g\gamma} - e^{-g}}{1 - e^{-g}} \tag{50}$$

and Dirichlet boundary conditions:

$$\begin{aligned} a(0, \tau) &= 1 \\ a(1, \tau) &= 0 \end{aligned} \tag{51}$$

By setting equation 49 equal to zero an analytical expression to the steady state problem can be found.
This yields

$$0 = \frac{d^2 a}{d\gamma^2} - \theta a. \tag{52}$$

From this the characteristic polynomial is given and eigenvalues can be found:

$$\begin{aligned} 0 &= \lambda^2 - \theta \\ \Rightarrow \lambda &= \pm\sqrt{\theta}. \end{aligned} \tag{53}$$

The general steady state solution, using the above eigenvalues, is:

$$a_{st}(\gamma) = C_1 e^{\sqrt{\theta}\gamma} + C_2 e^{-\sqrt{\theta}\gamma} \tag{54}$$

C_1 and C_2 is found by applying the boundary conditions

$$\begin{aligned} a_{st}(0) = 1 \quad &\Rightarrow \quad C_2 = 1 - C_1 \\ a_{st}(1) = 0 \quad &\Rightarrow \quad C_1 = -\tfrac{e^{-\sqrt{\theta}}}{2\sinh(\sqrt{\theta})} \end{aligned}$$

By rearranging and applying identity of sinh, the full solution to the steady state is given by:

$$a_{st}(\gamma) = \frac{\sinh(\sqrt{\theta}(1-\gamma))}{\sinh(\sqrt{\theta})}. \tag{55}$$

In Figure 5 equation 55 is plotted. θ determines how fast the concentration of a goes to zero as γ increases.
The steady steade and the initial condition is plotted together in Figure 6, showing that the steady state solution is fairly close to the initial condition. This means the system in itself does not move much away from the initial concentration given to the system.

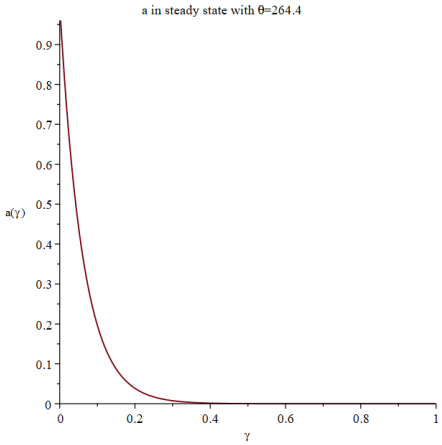

Figure 5: *a in steady state.* $\theta = 264.4$ *and dirichlet boundary conditions.*

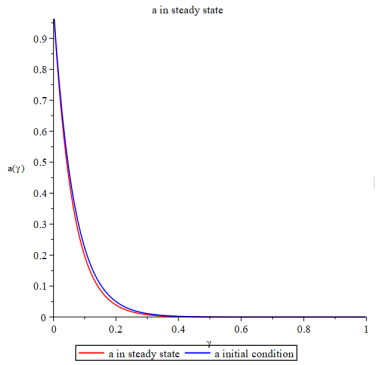

Figure 6: *a in steady state and the initial condition used to solve the system.*

Furthermore, numerical simulations show that with the dimensionless reaction rate $\theta = 264.4$, a fast convergence of a is observed. In Figure 7 the numerical solution as well as the analytical steady state solution is shown. The error is rather small for small τ, and is at approximately $\tau = 0.06$ seen beginning to go up, due to truncation errors being larger than the actual error between the two curves. This can be seen in Figure 7. It is seen to have converged convincingly at $\tau = 0.06$, which in our dimensional time is $t = 52.92$ days. On the timescale of the world, this is quite low, since we are interested on looking at timescales of centuries.

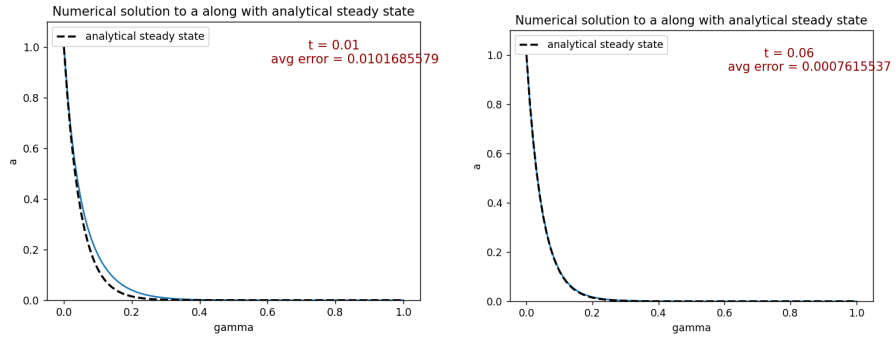

(a) *Numerical solution at* $\tau = 0.01$ (b) *Numerical solution at* $\tau = 0.06$

Figure 7: *Numerical solution converging to analytical steady state solution to* a

Numerical simulations show fast convergence to a steady state of a. This makes it reasonable to only utilize expression for the steady state in a, and effectively treat a as a forcing of b instead of a dynamical variable, as first intended. The full solution of a has been found by Fourier series, and the derivation is in appendix 11.2.

5 Steady state solution to b

Since our system is relevant over long time periods, it is reasonable to assume it will quickly reach a steady state, where the solution becomes invariant in time. This happens when transients of the system has died out. This is meaningful since the forcing of the system, the reaction term, is seen to quite quickly converge to a steady state. In section 4 it is seen how quickly the solution becomes constant in time. Because of this, the concentration of b will be subject to a constant forcing rather fast throughout time. This gives reason to ignore the transient phase and only focus on the steady state solutions to b as well.

Equation 16 can in a steady state be written as a non-homogeneous ODE:

$$\frac{d}{d\gamma}\left(\hat{d}_b\frac{db(\gamma)}{d\gamma}+\widehat{Pe_a}(\gamma)b(\gamma)\right)+\theta a_{st}(\gamma)=0. \tag{56}$$

Note that the reaction term $a(\tau,\gamma)$ has been replaced with the steady state solution $a_{st}(\gamma)$. Equation 56 can be expanded as

$$b''(\gamma)+\frac{\widehat{Pe_a}(\gamma)}{\hat{d}_b}b'(\gamma)+\frac{\widehat{Pe_a}'(\gamma)}{\hat{d}_b}b(\gamma)=-\frac{a_{st}(\gamma)}{\hat{d}_b}. \tag{57}$$

For the sake of simplicity let $\hat{d}_b=1$ to begin with. This will result in $\frac{1}{\hat{d}_b}$ to vanish from the model.
The above can be solved by assuming that the solution is a sum of the solution to the homogeneous part of the problem, disregarding the reaction term, and the solution to the inhomogeneous part (particular solution),

$$b(\gamma)=b_{hom}(\gamma)+b_{par}(\gamma), \tag{58}$$

5.1 Homogeneous part

The homogeneous part of our differential equation is:

$$b''_{hom}(\gamma)+\widehat{Pe_a}(\gamma)b'_{hom}(\gamma)+(\widehat{Pe_a})'(\gamma)b_{hom}(\gamma)=0, \tag{59}$$

with boundary conditions as defined in eq. 26 and $\hat{d}_b=1$.
The only solution to this is the trivial solution. This can be seen as the initial condition for b is 0-concentration on the entire domain. Because no forcing/source term is present, no b will ever by produced and the initial condition will remain as a steady state of the homogeneous part of the system. No b ever enters the system and therefore no b can ever be made, there is no gradient $b'=0$ and no acceleration $b''=0$ present for all τ.

$$b_{hom}(\gamma)\equiv 0. \tag{60}$$

From the above it is clear that the solution to the inhomogeneous component is a unique part of the overall solution. By Theorem 2, the particular solution b_{par} is guaranteed to be the unique solution of the differential equation given in (57), meaning $b(\gamma)=b_{par}(\gamma)$.

5.2 Inhomogeneous part

The inhomogeneous solution is found by solving:

$$b''(\gamma) + \widehat{Pe_a}(\gamma)b'(\gamma) + (\widehat{Pe_a})'(\gamma)b(\gamma) = -a_{st}(\gamma) \tag{61}$$

It can be solved by first collecting the three terms in 61 and introducing an integrating factor as such:

$$\begin{aligned}(b'(\gamma) + \widehat{Pe_a}(\gamma)b(\gamma))' &= -\phi(\gamma) \\ \Rightarrow b'(\gamma) + \widehat{Pe_a}(\gamma)b(\gamma) &= -\int_0^\gamma a_{st}(s)ds + C_1\end{aligned} \tag{62}$$

phi=a_st'

by boundary condition

$$b'(1) + \hat{Pe}_a(1)b(1) = 0 \tag{63}$$

OBS

yielding an implicit expression for C_1 which can be evaluated:

$$b'(1) + \hat{Pe}_a(1)b(1) = 0 \Rightarrow -\int_0^1 a_{st}(s)ds + C_1 = 0 \tag{64}$$

$$\Rightarrow C_1 = \int_0^1 a_{st}(s)ds \tag{65}$$

$$\begin{aligned}&\Rightarrow b'(\gamma) + \widehat{Pe_a}(\gamma)b(\gamma) = -\int_0^\gamma a_{st}(s)ds + \int_0^1 a_{st}(\gamma)d\gamma. \\ &\text{Multiplying by an integrating factor: } \mu(\gamma) = e^{\int_0^\gamma \widehat{Pe_a}(k)dk} \\ &\Rightarrow (b(\gamma)\mu(\gamma))' = \mu(\gamma)\Big(-\int_0^\gamma a_{st}(s)ds + \int_0^1 a_{st}(\gamma)d\gamma\Big) \\ &\Rightarrow b(\gamma) = \frac{1}{\mu(\gamma)}\int_0^\gamma \mu(\hat{s})\Big(-\int_0^\gamma a_{st}(s)ds + \int_0^1 a_{st}(\gamma)d\gamma\Big)d\hat{s} + C_2\end{aligned} \tag{66}$$

From the boundary condition $b(0) = 0$ we see that $C_2 = 0$.
This yields the final implicit form of the steady state solution for b:

$$b(\gamma) = \frac{1}{\mu(\gamma)}\int_0^\gamma \mu(\hat{s})\Big(-\int_0^\gamma a_{st}(s)ds + \int_0^1 a_{st}(\gamma)d\gamma\Big)d\hat{s} \tag{67}$$

This solution is unique, since only the trivial solution is a solution to the homogeneous case.
The way C_1 is determined here is unorthodox. Normally all integration constant are carried during all calculations and determined last. The solution in equation 67 can be written out explicitly and so can the derivative, to determine C_1, the calculations are however cumbersome.
Since the homogeneous part is trivial however, $b(\gamma) = b_{par}(\gamma)$, and no other parts need to be included in determining coefficients. It can be seen that C_1 could be carried through the calculations, finding $C_2 = 0$ and thus reverse all calculations back to eq.

62 and same argument could thus follow. Therefor in this specific case the expression for C_1 holds, however if $b_{hom} \neq 0$ this would be an invalid method of determining integration constants based on boundary conditions.

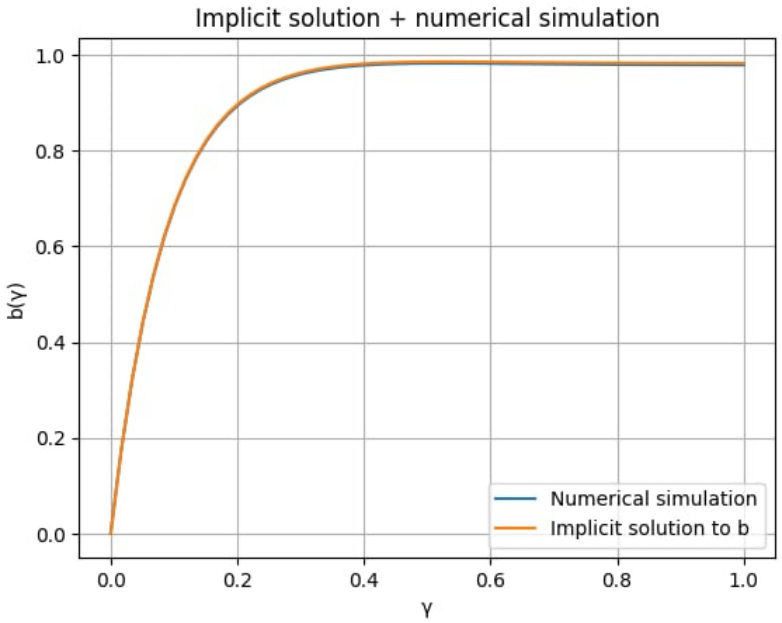

Figure 8: Implicit analytical solution for b steady state, plotted along with the numerical solution to the problem.

In Figure 8 the implicit solution is plotted together with a numerical solution to the problem. The two curves are seen aligning well only with a small deviation at the very end of the domain. A build up is seen forming and no difference is seen in the transition between water and sediment. This is arguably because no decay is included in the model, so a constant concentration of a at $\gamma = 0$ will be transformed into b, thus only b is being put in to the system and the zero-flux boundary ensures nothing leaves the system.

6 Power series solutions

To better understand the dynamics of the system, it has been chosen to expand the equations into power series. Even though an analytical implicit expression could be found for b in steady state, for future work, this expansion is beneficial. Especially if diffusion is also made spatially dependent in a further examination of this model.
Using the method of expanding into power series as outlined in section 3.1. This method is applicable since the problem only has varying coefficients that are all well-defined and analytical.
This method assumes a solution on the form:

$$b(\gamma) = \sum_{n=0}^{\infty} a_n \gamma^n. \tag{68}$$

Where the coefficients a_n are determined recursively relating to a_0 and a_1 found by inferring the boundary conditions.
By differentiating the assumed solution in eq. 68, and shifting the sums, the solution can be written up, but first the differentials

$$b'(\gamma) = \sum_{n=1}^{\infty} n a_n \gamma^{n-1} = \sum_{n=0}^{\infty} n(n+1) a_{n+1} \gamma^n, \tag{69}$$

$$b''(\gamma) = \sum_{n=2}^{\infty} n(n-1) a_n \gamma^{n-2} = \sum_{n=0}^{\infty} (n+2)(n+1) a_{n+2} \gamma^n. \tag{70}$$

The force term $\theta a_{st}(\gamma)$ is written out as a sum:

$$\theta a_{st}(\gamma) = \theta \frac{\sinh(\sqrt{\theta}(1-\gamma))}{\sinh(\sqrt{\theta})} = \sum_{n=0}^{\infty} \gamma^n \theta \left(\frac{e^{\sqrt{\theta}}}{2\sinh\sqrt{\theta}} \frac{(-\sqrt{\theta})^n}{n!} - \frac{e^{-\sqrt{\theta}}}{2\sinh\sqrt{\theta}} \frac{\sqrt{\theta}^n}{n!} \right). \tag{71}$$

In order to properly investigate the power series solution as posed above, four different cases will be considered.

- **Case 1:** Letting $\hat{d}_b = 1$.
- **Case 2:** Letting $\hat{d}_b = 1 + \epsilon$.
- **Case 3:** Letting $b(0)$ be non-zero, δ.
- **Case 4:** Allowing the homogeneous part of the solution to be non-zero.

6.1 Case 1

For case 1: $\hat{d_b} = 1$ again, equation 59 can be rewritten into a power series as such that

$$\begin{aligned}&\sum_{n=0}^{\infty}(n+2)(n+1)a_{n+2}\gamma^n + \widehat{Pe_a}(\gamma)\sum_{n=0}^{\infty}n(n+1)a_{n+1}\gamma^n + \widehat{Pe_a}'(\gamma)\sum_{n=0}^{\infty}a_n\gamma^n \\ &= -\sum_{n=0}^{\infty}\gamma^n\theta\bigg(\frac{e^{\sqrt{\theta}}}{2\sinh\sqrt{\theta}}\frac{(-\sqrt{\theta})^n}{n!} - \frac{e^{-\sqrt{\theta}}}{2\sinh\sqrt{\theta}}\frac{\sqrt{\theta}^n}{n!}\bigg).\end{aligned} \tag{72}$$

where

$$\begin{aligned}A &= \theta\frac{e^{\sqrt{\theta}}}{2\sinh\sqrt{\theta}}, \\ B &= \theta\frac{e^{-\sqrt{\theta}}}{2\sinh\sqrt{\theta}}.\end{aligned}$$

Where A, B are not to be confused with the concentrations of the particles from the original model with dimensions.
This can be simplified by taking γ^n out of a parenthesis and collecting on one sum over n's:

$$\sum_{n=0}^{\infty}\gamma^n\bigg((n+2)(n+1)a_{n+2}+\widehat{Pe_a}(\gamma)n(n+1)a_{n+1}+(\widehat{Pe_a})'(\gamma)a_n-(A\frac{(-\sqrt{\theta})^n}{n!}-B\frac{\sqrt{\theta}^n}{n!})\bigg) = 0. \tag{73}$$

The polynomials $\widehat{Pe_a}(\gamma)$ and $(\widehat{Pe_a})'(\gamma)$ can also be written as sums:

$$\begin{aligned}\widehat{Pe_a}(\gamma) &= \sum_{k=0}^{4}\widehat{Pe_a}_k\gamma^k \\ (\widehat{Pe_a})'(\gamma) &= \sum_{k=0}^{3}(\widehat{Pe_a})'_k\gamma^k\end{aligned} \tag{74}$$

where $\widehat{Pea}_k$ and $(\widehat{Pe_a})'_k$ denotes the k'th degree coefficient in the polynomials. It can now be inserted and collected on one sum:

$$\sum_{n=0}^{\infty}\gamma^n\bigg((n+2)(n+1)a_{n+2} + \sum_{k=0}^{k=4}\widehat{Pe_a}_k n(n-k+1)a_{n-k+1} + \sum_{k=0}^{k=3}(\widehat{Pe_a})'_k a_{n-k} - (A\frac{(-\sqrt{\theta})^n}{n!} - B\frac{\sqrt{\theta}^n}{n!})\bigg) = 0 \tag{75}$$

The coefficients a_n are found by setting the parenthesis to equal 0 and isolating a_{n+2}. a_0 and a_1 are found by the boundary conditions and the rest found recursively using these two.

$$a_{n+2} = -\frac{1}{(n+2)(n+1)}\bigg(\sum_{k=0}^{k=4}\widehat{Pe_a}_k n(n-k+1)a_{n-k+1}+\sum_{k=0}^{k=3}(\widehat{Pe_a})'_k a_{n-k}-(A\frac{(-\sqrt{\theta})^n}{n!}-B\frac{\sqrt{\theta}^n}{n!})\bigg) \tag{76}$$

For this recursive relationship to hold the following must be defined

$$a_m = 0 \text{ if } m < 0. \tag{77}$$

Applying the Dirichlet boundary condition, $b(0) = 0$, on equation 68 a_0 can be found as

$$b(0) = \sum_{n=0}^{\infty} a_n 0^n = a_0 = 0. \tag{78}$$

From this we know that the coefficients must be dependent solely on a_1, which is to be inferred from the second boundary condition. Assuming that the equation 68 can be split into a homogeneous and inhomogeneous part and that each can be written as a power series, by assuming the relation

$$a_n = a_1 c_n + d_n \tag{79}$$

then it follows that

sum om alt og gamma()

$$b(\gamma) = \left(a_1 \sum_{n=0}^{\infty} c_n + \sum_{n=0}^{\infty} d_n \right) \gamma^n, \tag{80}$$

where $a_1 c_n$ is the part determined by the homogeneous system and d_n is the part determined by the inhomogeneous system. By inspecting equation 76 and inserting the relation into equation 80, c_n and d_n can be written out as

$$\begin{aligned} c_{n+2} &= -\frac{1}{(n+2)(n+1)} \left(\sum_{k=0}^{k=4} \widehat{Pe_a}_k n(n-k+1) c_{n-k+1} + \sum_{k=0}^{k=3} (\widehat{Pe_a})'_k c_{n-k} \right) \\ d_{n+2} &= -\frac{1}{(n+2)(n+1)} \left(\sum_{k=0}^{k=4} \widehat{Pe_a}_k n(n-k+1) d_{n-k+1} + \sum_{k=0}^{k=3} (\widehat{Pe_a})'_k d_{n-k} - (A\frac{(-\sqrt{\theta})^n}{n!} - B\frac{\sqrt{\theta}^n}{n!}) \right) \end{aligned} \tag{81}$$

where

$$c_n = 0 \text{ and } d_n = 0 \text{ if } n < 0 \tag{82}$$

As shown in section 5.1, the only solution to the homogeneous system is the trivial. Then it follows by assumption that $\forall n : c_n = 0$. As a consequence a_1 is not a free parameter and the solution will be purely determined by $\sum_{n=0}^{\infty} d_n$. Then by assumption the first two parameter in the recurrence relation for c and d we have

$$\begin{aligned} &c_0 = 0,\ c_1 = 0 \\ &d_0 = 0,\ d_1 \in \{\mathcal{R}^+ \wedge 0\}. \end{aligned} \tag{83}$$

This gives 2 cases:

- case 1.1: $d_1 = 0$

- case 1.2: $d_1 \in \mathcal{R}^+$

either d_1 is zero and only d_n terms of $n \geq 2$ will be contributing to the solution, or d_1 is a free parameter used for tuning to the second boundary condition.

6.1.1 Case 1.1

The full solution to the problem in case 1.1 is:

Power series solution to b in steady state, case 1.1:

$$b(\gamma) = \sum_{n=0}^{\infty} d_n \gamma^n$$

with

$$a_0 = 0 \Rightarrow d_0 = 0$$

$$a_1 = 0 \Rightarrow d_1 = 0$$

$$d_{n+2} = -\frac{1}{(n+2)(n+1)}\left(\sum_{k=0}^{k=4} \widehat{Pe_a}_k n(n-k+1)d_{n-k+1} + \sum_{k=0}^{k=3} (\widehat{Pe_a})'_k d_{n-k} - (A\frac{(-\sqrt{\theta})^n}{n!} - B\frac{\sqrt{\theta}^n}{n!})\right) \tag{84}$$

Since a a degree of freedom is lost because a_1 cannot be determined with of use of the second boundary condition, a some-what degenerative case problem arises, when solving with the power series method. Since it is impossible to force a second boundary condition on the system, the solution cannot be "stopped" specified end of the domain, in this case at $\gamma = 1$.

The coefficients of the power series solutions are plotted in Figure 9. The coefficients converge which implies that only a few terms in a truncated sum are needed in order to graphically represent the solution. At around $n = 10$ the largest magnitude of coefficients are found and after approximately $n = 25$ settle around 0. All figures showing solutions obtained by series solutions will be truncated at $N = 100$ to ensure that coefficients have converged sufficiently.

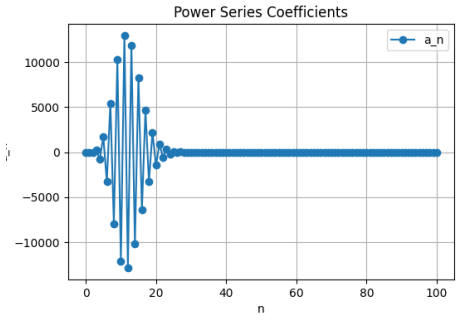

Figure 9: *Coefficients $a_n = d_n$ for power series solution of $b(\gamma)$, case 1.1, truncated from N=100 terms.*

Using truncated sum up to $N = 100$ we get the coefficients to the power series as seen plotted in Figure 10.

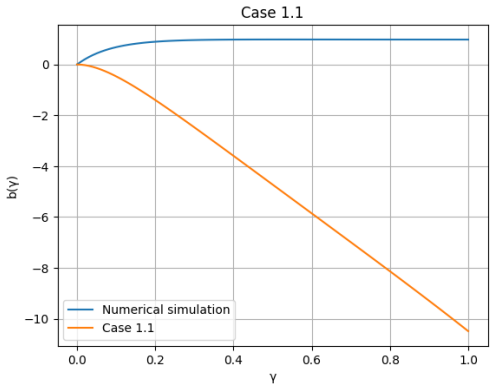

Figure 10: *The concentration of the dimensionless concentration of particles of type B in steady state, case 1.1, solved analytically, using truncated sums with 100 terms. Plotted along the numerical solution.*

The solution has negative concentrations and is no longer restricted to the domain of $\gamma = [0; 1]$ since the bottom boundary condition is not possible to hold. The system solution is seen to be only dependent on the reaction term. It is plotted together with a numerical simulation of the solution to compare.

6.1.2 Case 1.2

When allowing d_1 to be a free parameter, its value can be tuned to adhere to the second boundary condition, thus restricting the domain and ensuring sensible concentrations. The boundary condition

$$b'(1) + \widehat{Pe_a}(1)b(1) = 0 \tag{85}$$

is introduced by rewriting it to power series:

$$\begin{aligned} b(\gamma) &= \sum_{n=0}^{\infty} d_n \gamma^n \\ b(1) &= \sum_{n=0}^{\infty} d_n \\ b'(\gamma) &= \sum_{n=1}^{\infty} n d_n \gamma^{n-1} \\ b'(1) &= \sum_{n=1}^{\infty} n d_n \end{aligned} \tag{86}$$

Thus the BC yields:

$$\sum_{n=1}^{\infty} n d_n + \widehat{Pe_a}(1) \sum_{n=0}^{\infty} d_n = 0 \tag{87}$$

using $d_0 = 0$ and isolating d_1 yields

$$d_1 = -\frac{\sum_{n=2}^{\infty} n d_n - \widehat{Pe_a}(1) \sum_{n=2}^{\infty} d_n}{1 + \widehat{Pe_a}(1)} \tag{88}$$

The solution to case 1.2 is

Power series solution to b in steady state, case 1.2:

$$\begin{aligned} &b(\gamma) = \sum_{n=0}^{\infty} d_n \gamma^n \\ &\text{with} \\ &a_0 = 0 \Rightarrow d_0 = 0 \\ &a_1 = 0 \Rightarrow d_1 = \mathcal{R} \\ &d_1 = -\frac{\sum_{n=2}^{\infty} n d_n - \widehat{Pe_a}(1) \sum_{n=2}^{\infty} d_n}{1 + \widehat{Pe_a}(1)} \\ &d_{n+2} = -\frac{1}{(n+2)(n+1)} \Bigg(\sum_{k=0}^{k=4} \widehat{Pe_a}_k n(n-k+1) d_{n-k+1} \\ &+ \sum_{k=0}^{k=3} (\widehat{Pe_a})'_k d_{n-k} - (A \frac{(-\sqrt{\theta})^n}{n!} - B \frac{\sqrt{\theta}^n}{n!}) \Bigg) \end{aligned} \tag{89}$$

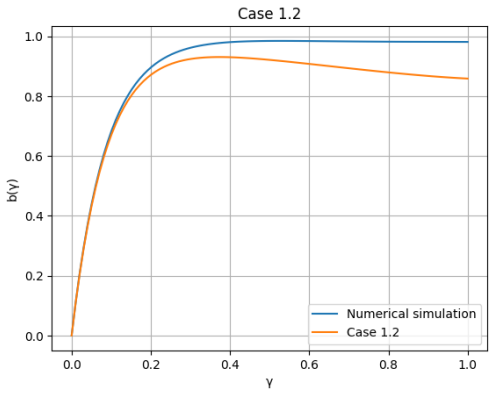

Figure 11: *Concentration of b in steady state from case 1.2, using truncated sums up to $N = 100$ terms plotted along with a numerical solution.*

By this method of estimating d_1 to fit the second boundary condition, the coefficient value is found to be $d_1 = 11.3757$.
The power series solution is plotted in Figure 11. Here the concentration of b is positive, between 0 and 1. For small γs the solution follows the numerical simulation nicely but it deviates quickly. This is a sign that the same solutions are not found by these two methods. This could be because there are infinitely many solutions to the problem, and the numerics are just choosing one arbitrarily.

6.2 Case 2: Perturbation of the operator

After seeing that case 1.2 is in fact sensible in concentrations but does not match numerics, another case is examined. This keeps d_1 as a free parameter as in case 1.2 but imposes a perturbation on the diffusion, $\hat{d}_b = 1 + \epsilon$ is determined and examined. Solving by power series method as done in previous sections, a new term for a_{n+2} is found to be:

$$a_{n+2} = -\frac{1}{(n+2)(n+1)(1+\epsilon)}\left(\sum_{k=0}^{k=4}\widehat{Pe_a}_k n(n-k+1)a_{n-k+1}+\sum_{k=0}^{k=3}(\widehat{Pe_a})'_k a_{n-k}-(A\frac{(-\sqrt{\theta})^n}{n!}-B\frac{\sqrt{\theta}^n}{n!})\right) \tag{90}$$

This can, as in previous section, be written as a linear recurrence relation with a_1 since the boundary condition $b(0) = 0$ will yield $a_0 = 0$. However with the chosen initial condition and boundary conditions, it will still only have the trivial solution to the homogeneous equation. Again the system will gain its degree of freedom given by d_1.

The final power series solution for case 2 is:

Power series solution to b in steady state, case 2:

$$b(\gamma) = (a_1\sum_{n=0}^{\infty}c_n + \sum_{n=0}^{\infty}d_n)\gamma^n$$

with

$$a_0 = 0 \Rightarrow c_0 = 0,\ d_0 = 0$$

$$a_1 = 0 \Rightarrow c_1 = 0,\ d_1 = \mathcal{R}$$

$$d_1 = -\frac{\sum_{n=2}^{\infty} n d_n - \widehat{Pe_a}(1)\sum_{n=2}^{\infty} d_n}{1+\widehat{Pe_a}(1)}$$

$$d_{n+2} = -\frac{1}{(n+2)(n+1)(1+\epsilon)}\left(\sum_{k=0}^{4}\widehat{Pe_a}_k\, n(n-k+1)d_{n-k+1}\right.$$

$$\left.+\sum_{k=0}^{3}(\widehat{Pe_a})'_k\, d_{n-k} - \left(A\frac{(-\sqrt{\theta})^n}{n!} - B\frac{\sqrt{\theta}^n}{n!}\right)\right)$$

(91)

The imposed perturbation is a regular perturbation, as it does not change the qualitative behavior of the solutions. Solutions are almost identical to solutions found in case 1.2. Below the new solution is shown along with the coefficients plotted in Figure 12. The concentration of b from of case 2 can be seen in Figure 13, which as expected, does not differ much from case 1.2. Ones again the perturbation does not entail the same solution as numerical simulations do.

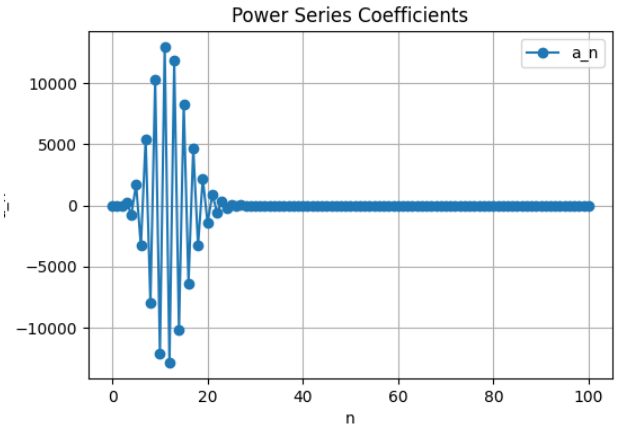

Figure 12: *Coefficients $a_n = d_n$ for power series solution of $b(\gamma)$, case 2, truncated from N=100 terms.*

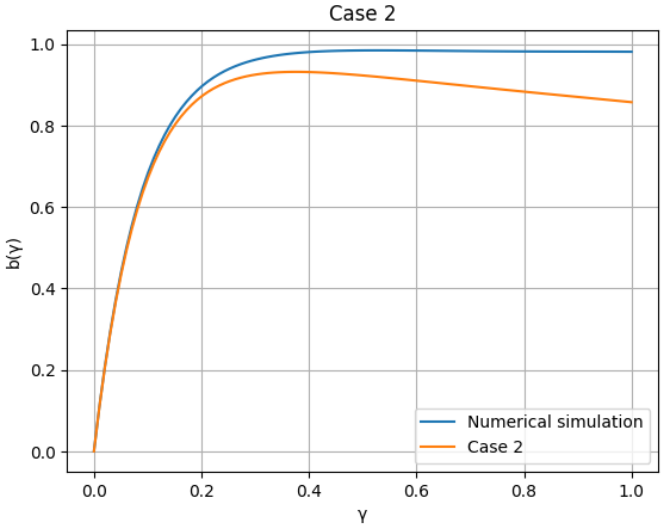

Figure 13: *The concentration of the dimensionless concentration of particles of type B in steady state, case 2, solved analytically, using truncated sums with 100 terms and using $\epsilon = 10^{-10}$. Plotted along the numerical solution.*

6.3 Case 3: Perturbation of the boundary conditions

Another way to ensure the system avoids being overconstraint by two boundary conditions, is to allow the dirichlet boundary condition to become non-zero. Then when utilizing the relation, $a_n = a_n c_n + d_n$, c_n is allowed to be non-zero. This in turn means

a1

that a_1 becomes a free parameter. By perturbating the Dirichlet boundary condition it ensures that the trivial solution won't be the only solution to the homogeneous part. By gaining a free a parameter the degenerateness is combated and the free parameter can be tuned to fit the second boundary condition. For simplicity we choose $\hat{d_b} = 1$ since relative diffusion does not have a large impact on the dynamics of the system.

Perturbed boundary conditions:

$$b(0) = \delta, \qquad J_b(1) = 0, \tag{92}$$

where J_b is the flux and defined as

$$J_b(\gamma) = b'(\gamma) + \widehat{Pe}_a(\gamma)\, b(\gamma). \tag{93}$$

This perturbation is of the original system since as $\delta \to 0$ the original system is recovered. The new boundary conditions given in equation 92 does not change the derivation of the power series from that of case 1, therefore the same expression arises and the coefficients are expressed by the recurrence relation

$$a_{n+2} = -\frac{1}{(n+2)(n+1)}\left(\sum_{k=0}^{k=4} \widehat{Pe}_{a_k} n(n-k+1)a_{n-k+1} + \sum_{k=0}^{k=3} (\widehat{Pe}_a)'_k a_{n-k} - (A\frac{(-\sqrt{\theta})^n}{n!} - B\frac{\sqrt{\theta}^n}{n!})\right). \tag{94}$$

But, applying the boundary conditions to eq. 68 and 69 it yields

$$a_0 = \delta. \tag{95}$$

This is an auxiliary value and ensures an extra degree of freedom such that adhering to the second boundary condition is possible. This makes a_0 a free parameter instead of d_1 or a_1, as seen in earlier cases. The coefficients can again be expressed as a linear dependency on one parameter, this time $a_0 = \delta$. The coefficients can be written as:

$$\sum_{n=0}^{\infty} a_n = \delta \sum_{n=0}^{\infty} c_n + \sum_{n=0}^{\infty} d_n \tag{96}$$

where δ can be found by inserting eq.68 and 69 into the no-flux boundary condition and isolating.

$$\delta = \frac{\sum_{n=0}^{\infty} n d_n + \widehat{Pe_a}(1) \sum_{n=0}^{\infty} d_n}{\sum_{n=0}^{\infty} n c_n + \widehat{Pe_a}(1) \sum_{n=0}^{\infty} c_n}. \tag{97}$$

This will be the perturbation value needed that upholds the boundary condition. Since the homogeneous solution space is not only the trivial solution, uniqueness is not guaranteed.

The power series solution for case 3 is:

Power series solution to b in steady state, case 3:

$$b(\gamma) = (a_0 \sum_{n=0}^{\infty} c_n + \sum_{n=0}^{\infty} d_n)\gamma^n$$

with

$$a_0 = \delta \Rightarrow c_0 = 0,\ d_0 = \delta$$

$$a_1 = a_0 c_1 + d_1 \Rightarrow d_1 = 0,\ c_1 = 1,\ a_1 = a_0$$

$$\delta = \frac{\sum_{n=0}^{\infty} n d_n + \widehat{Pe_a}(1) \sum_{n=0}^{\infty} d_n}{\sum_{n=0}^{\infty} n c_n + \widehat{Pe_a}(1) \sum_{n=0}^{\infty} c_n} \tag{98}$$

$$c_{n+2} = -\frac{1}{(n+2)(n+1)} \left(\sum_{k=0}^{4} \widehat{Pe_a}_k n(n-k+1) c_{n-k+1} + \sum_{k=0}^{3} (\widehat{Pe_a})'_k c_{n-k} \right)$$

$$d_{n+2} = -\frac{1}{(n+2)(n+1)} \left(\sum_{k=0}^{4} \widehat{Pe_a}_k n(n-k+1) d_{n-k+1} \right.$$

$$\left. + \sum_{k=0}^{3} (\widehat{Pe_a})'_k d_{n-k} - (A\frac{(-\sqrt{\theta})^n}{n!} - B\frac{\sqrt{\theta}^n}{n!}) \right)$$

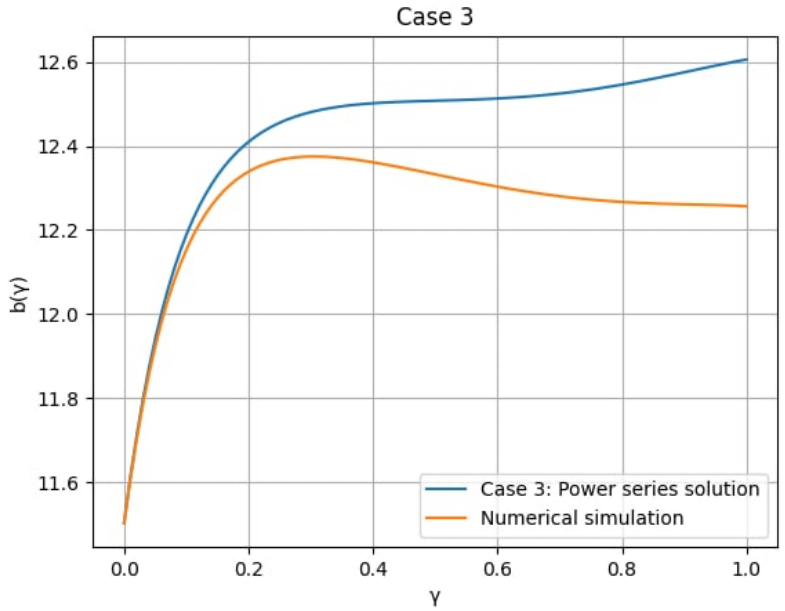

Figure 14: *Power series solution of concentration of b in steady state, truncated at* $N = 100$ *terms, plotted along with the numerical solution of the same problem.*

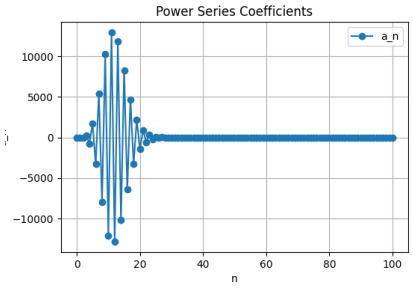

(a) *Power series coefficients* a_n

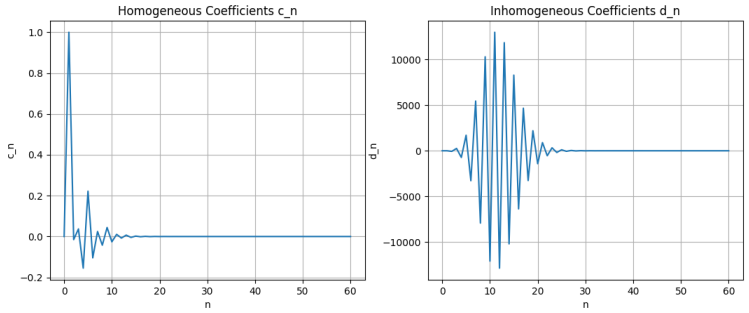

(b) *Power series coefficients components*

Figure 15: *The coefficients* a_n *and it's components, the component representing the homogeneous part* c_n *and the component representing the inhomogeneous part* d_n*. Sums truncated at* $N = 100$ *terms.*

For the boundary conditions to be held, a δ-value is found, which is needed for the boundary condition at $\gamma = 1$ to be held. The found value, with truncation at $N = 100$ terms in the sums are:

$$\delta = \frac{\sum_{n=0}^{\infty} nd_n + \widehat{Pe_a}(1) \sum_{n=0}^{\infty} d_n}{\sum_{n=0}^{\infty} nc_n + \widehat{Pe_a}(1) \sum_{n=0}^{\infty} c_n} = 11.502 \tag{99}$$

which results in an absolute error on the zero-flux robin boundary condition of $-5.697 \cdot 10^{-11}$. This can be attributed to truncation errors mostly from the power series and from the numerical simulations. The value of the auxiliary value should not be interpreted as a concentration per say but more like a measure of how incompatible our model is with the 2 boundary conditions posed.

6.4 Case 4: Perturbation of homogeneous solution

A numerical experiment was carried out, to hopefully be able to uphold all boundary conditions and match the numerical simulations with a kind of perturbation.
We now allow $c_n \neq 0$ instead of $c_n = 0$. The few transient terms, as seen in Figure 16, to tune the solution such that is fits with both boundary conditions:

$$b'(1) + \rho(1)b(1) = 0 \tag{100}$$

From the derivation of the power series we know that $a_0 = 0$, and that the linear dependency $a_0 = a_1 c_0 + d_0 = 0$ holds, and thus $c_0 = d_0 = 0$. Now, we will no longer force $c_1 = 0$ and let other solutions than the trivial for the homogeneous case to exists.

$$\begin{aligned} a_1 &= a_1 c_1 + d_1 \\ &\Rightarrow d_1 = 0 \\ &\Rightarrow c_1 = 1 \end{aligned} \tag{101}$$

This, again, allows a_1 to be a free parameter, while still adhering to the Dirichlet boundary condition $b(0) = 0$. This is done by substituting the power series into equation 100:

$$\begin{aligned} b(1) &= \sum_{n=0}^{\infty} a_n = a_1 \sum_{n=0}^{\infty} c_n + \sum_{n=0}^{\infty} d_n \\ b'(1) &= \sum_{n=0}^{\infty} n a_n = a_1 \sum_{n=0}^{\infty} n c_n + \sum_{n=0}^{\infty} n d_n \end{aligned} \tag{102}$$

Inserting into the robin boundary condition:

$$\begin{aligned} & a_1 \sum_{n=0}^{\infty} n c_n + \sum_{n=0}^{\infty} n d_n + \rho(1)(a_1 \sum_{n=0}^{\infty} c_n + \sum_{n=0}^{\infty} d_n) = 0 \\ \Rightarrow\ & a_1 = \frac{\sum_{n=0}^{\infty} n d_n + \rho(1) \sum_{n=0}^{\infty} d_n}{\sum_{n=0}^{\infty} n c_n + \rho(1) \sum_{n=0}^{\infty} c_n}. \end{aligned} \tag{103}$$

This allows a_1 to be a free parameter and permits the solution adhere to the second boundary condition. When perturbing the other boundary condition in case 3, it is clear from, Figure 15b, that the first coefficients in c_n takes the same values.

Power series solution to b in steady state, case 4:

$$b(\gamma) = (a_1 \sum_{n=0}^{\infty} c_n + \sum_{n=0}^{\infty} d_n)\gamma^n$$

with

$$a_0 = 0 \Rightarrow c_0 = 0,\ d_0 = 0$$

$$a_1 = a_1 c_1 + d_1 \Rightarrow c_1 = 1,\ d_1 = 0,\ a_1 \in \mathcal{R}$$

$$a_1 = \frac{\sum_{n=0}^{\infty} n d_n + \widehat{Pe_a}(1) \sum_{n=0}^{\infty} d_n}{\sum_{n=0}^{\infty} n c_n + \widehat{Pe_a}(1) \sum_{n=0}^{\infty} c_n} \tag{104}$$

$$c_{n+2} = -\frac{1}{(n+2)(n+1)} \left(\sum_{k=0}^{4} \widehat{Pe_a}_k n(n-k+1) c_{n-k+1} + \sum_{k=0}^{3} (\widehat{Pe_a})'_k c_{n-k} \right)$$

$$d_{n+2} = -\frac{1}{(n+2)(n+1)} \left(\sum_{k=0}^{4} \widehat{Pe_a}_k n(n-k+1) d_{n-k+1} + \right.$$

$$\left. \sum_{k=0}^{3} (\widehat{Pe_a})'_k d_{n-k} - (A \frac{(-\sqrt{\theta})^n}{n!} - B \frac{\sqrt{\theta}^n}{n!}) \right)$$

This solution resembles case 3, however it still upholds the boundary condition of $b(0) = 0$. The coefficients of this solution can be seen in Figure 16. $c_1 = 1$ is clearly the most impactfull coefficient. However, the magnitude of the coefficients for the homogeneous part are much smaller than coefficients for the inhomogeneous part, d_n. This still shows that the reaction term has a large impact on the solution, but the small transient phase in the homogeneous solution allows boundary conditions to be held.

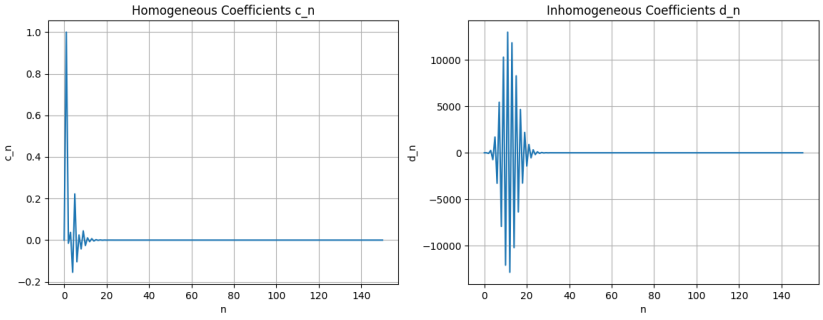

Figure 16: *Coefficient components from case 4*

In Figure 17 the solution truncated at $N = 100$ terms, is plotted alongside a numerical simulation. The solutions clearly overlap.
In Figure 18 as N increases the solution settles and begin resembling both the numerical simulation and the implicit solution (Figure 8).

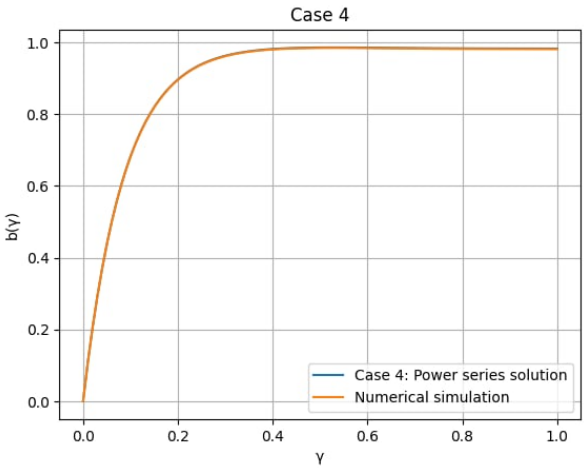

Figure 17: *Solution to the steady state of b using power series solutions to case 4. Plotted along with the numerical simulation to the problem.*

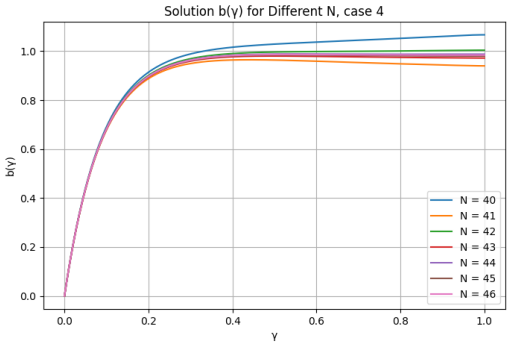

Figure 18: *Steady state solution to the concentration of b, using power series method with truncated sum up to different number of terms N.*

7 Sturm Liouville formulation of steady state problem in b

For the sake of analyzing equations 24 and 25 using Sturm Liouville theory, the problem is rewritten to Sturm-Liouville form. This is done since a self-adjoint Sturm-Liouville form will guarantee several useful properties and might explain why the power series method is not meaningful for the case where $\hat{d}_b = 1$. Now let $a(\tau, \gamma)$ be in steady state, divide through with $\hat{d}_b$ and let $\partial b/\partial \tau = 0$ then the resulting equation can be seen in 57. Defining the corresponding eigenvalue problem for equation 57 yields

$$\frac{d^2b}{d\gamma^2} + \frac{\widehat{Pe_a}(\gamma)}{\hat{d}_b}\frac{db}{d\gamma} + \frac{(\widehat{Pe_a})'(\gamma)}{\hat{d}_b}b = -\lambda b. \tag{105}$$

Even though a solution is found already, we are curious to see what properties may be inherited by interpreting the general form of the operator. By introducing a general form of the integrating factor used in earlier sections, equation 105 can be rewritten in Sturm Liouville form as such:

$$\begin{aligned}(\mu(\gamma)b')' + q(\gamma)b &= -\lambda b\mu(\gamma),\\ \mu(\gamma) &= e^{\int \frac{\widehat{Pe_a}(\gamma)}{\hat{d}_b}d\gamma},\\ q(\gamma) &= \mu(\gamma)\frac{(\widehat{Pe_a})'(\gamma)}{\hat{d}_b}.\end{aligned} \tag{106}$$

From the above the S-L operator revels itself as

$$\mathcal{L}_b = \frac{d}{d\gamma}\mu(\gamma)\frac{d}{d\gamma} + q(\gamma). \tag{107}$$

The eigenvalue problem for the S-L problem then becomes

$$\mathcal{L}_b[b] = -\lambda b\mu(\gamma). \tag{108}$$

From the above the weight function of the S-L problem can be seen as $\mu(\gamma)$, when comparing to equation 37.

For the remainder of this section the three cases will be examined

Case 1: $\hat{d}_b = 1$

Case 2: $\hat{d}_b = 1 + \epsilon$

Case 3: $\hat{d}_b = 1$ and $b(0) = \delta$

7.1 Case 1: The regular problem

Let $\hat{d_b} = 1$, and expand the operator in equation 107 then

$$\mathcal{L}_b = \frac{d^2}{d\gamma^2} + \widehat{Pe_a}(\gamma)\frac{d}{d\gamma} + (\widehat{Pe_a})'(\gamma). \tag{109}$$

To see if the operator self-adjoint, the properties listed in equations 40 are checked. It is easy to see that 2) is held since $p(x)$ in this case is $\mu(\gamma)$, which is analytical, well-defined and always strictly positive. To check if the operator is self-adjoint in 1) of equation 40 it is checked whether

$$\langle \mathcal{L}[u], v\rangle - \langle u, \mathcal{L}[v]\rangle = 0, \tag{110}$$

is true. This is done by using the definition of inner product in equation 41. Here $u(\gamma)$ and $v(\gamma)$ are arbitrary functions fulfilling the boundary conditions in equation 26. Since we only deal with real valued functions $u^* = u$, $v^* = v$, $\mathcal{L}[u]^* = \mathcal{L}[u]$ and $\mathcal{L}[v]^* = \mathcal{L}[v]$. The spatial dependency will not be written for this derivation, it is implied that all are functions of γ.

$$\begin{aligned}
&\langle \mathcal{L}[u], v\rangle - \langle u, \mathcal{L}[v]\rangle \\
=&\int_0^1 \mathcal{L}[u]v - u\mathcal{L}[v]d\gamma \\
=&\int_0^1 (u'' + \widehat{Pe_a}u' + (\widehat{Pe_a})'u)v - u(v'' + \widehat{Pe_a}v' + (\widehat{Pe_a})'v)d\gamma \\
=&\int_0^1 vu'' + v\widehat{Pe_a}u' + (\widehat{Pe_a})'uv - uv'' - u\hat{Pe_a}v' - u(\widehat{Pe_a})'vd\gamma \\
=&\int_0^1 vu'' + \widehat{Pe_a}vu' - uv'' - \widehat{Pe_a}uv'd\gamma \\
=&\int_0^1 (u'v - uv')'d\gamma + \int_0^1 \widehat{Pe_a}(v'u - uv')d\gamma \\
&\text{using integration by parts} \\
=&[\widehat{Pe_a}uv]_0^1 - \int_0^1 u(\widehat{Pe_a}v)'d\gamma - [\widehat{Pe_a}uv]_0^1 + \int_0^1 u(v'\widehat{Pe_a})'d\gamma
\end{aligned} \tag{111}$$

Now we apply the boundary conditions to u and v:

$$\begin{aligned}
&\text{at } \gamma = 0 : b(0) = 0, \\
&\Rightarrow \qquad u(0) = 0, v(0) = 0. \\
&\text{at } \gamma = 1 : b'(1) + \widehat{Pe_a}(1)b(1) = 0, \\
&\Rightarrow \qquad u'(1) + \widehat{Pe_a}(1)u(1) = 0, \\
&\qquad\qquad v'(1) + \widehat{Pe_a}(1)v(1) = 0.
\end{aligned} \tag{112}$$

and insert it into the expression:

$$\int_0^1 u(\widehat{Pe_a}v)' - u(v'\widehat{Pe_a})' d\gamma \neq 0 \tag{113}$$

The above is not equal zero since it has a second order differential in the term, not existing in the boundary conditions.
As a consequence the operator is not self-adjoint, and no properties of the Sturm-Liouville theory can be applied to our problem. Eigenvalues may be complex, eigenfunctions not necessarily orthogonal w.r.t the weight functions, and the solutions can be extremely sensitive to perturbations.

7.2 Case 2: Perturbation in diffusion

We now define a second case with $\hat{d}_b = 1 + \epsilon$, where $0 < \epsilon << 1$. This constitutes a regular perturbation, since it does not change the form of the operator or any of the qualitative behaviors of the system [Hansen] [**?**].
Here the perturbation parameter ϵ is multiplied onto the diffusive term. This is done to the diffusive term, since adding to the other terms, might entail us to make a position dependent perturbation.
The new model thus becomes:

$$(1+\epsilon)b''(\gamma) + \widehat{Pe_a}(\gamma)b'(\gamma) + \eta(\gamma)b(\gamma) = 0, \tag{114}$$

neta: pea'

with boundary conditions as defined in eq. 26.
This problem can be written as an eigenvalue problem on Sturm-Liouville form as equation 37:

$$\begin{aligned}
&(1+\epsilon)b'' + (\widehat{Pe_a}(\gamma)b)' = \lambda b \\
&\Rightarrow (1+\epsilon)b'' + (\widehat{Pe_a})'(\gamma)b + \widehat{Pe_a}(\gamma)b' = \lambda b \\
&\Rightarrow b'' + \frac{(\widehat{Pe_a})'(\gamma)}{1+\epsilon}b' + \frac{\widehat{Pe_a}(\gamma)}{1+\epsilon}b = \frac{\lambda}{1+\epsilon}b \qquad \text{mærke byttet} \\
&\text{defining } \hat{\lambda} = \frac{\lambda}{1+\epsilon} \\
&\Rightarrow b'' + \frac{(\widehat{Pe_a})'(\gamma)}{1+\epsilon}b' + \frac{\widehat{Pe_a}(\gamma)}{1+\epsilon}b = \hat{\lambda}b
\end{aligned}$$

multiplying by integrating factor $\mu(\gamma) = e^{\int_0^\gamma \frac{\widehat{Pe_a}(s)}{1+\epsilon}ds}$

$$\begin{aligned}
&\mu(\gamma)b'' + \mu(\gamma)\frac{(\widehat{Pe_a})'(\gamma)}{1+\epsilon}b' + \mu(\gamma)\frac{\widehat{Pe_a}(\gamma)}{1+\epsilon}b = \mu(\gamma)\hat{\lambda}b \\
&\Rightarrow (\mu(\gamma)b')' = \hat{\lambda}\mu(\gamma)b \qquad \text{since mu' = brøk}
\end{aligned} \tag{115}$$

The operator can be written out to

$$\mathcal{L}_\epsilon = \frac{d}{d\gamma}\mu\frac{d}{d\gamma} + q(\gamma) \tag{116}$$

with $q(\gamma) = \mu(\gamma)\frac{(\widehat{Pe_a})'(\gamma)}{1+\epsilon}$.
We can now check to see if the operator is in fact self-adjoint by checking the criteria as mentioned in equation 40. By the same argument as in case 1, and since $\epsilon \neq 0$, it is seen that criteria 2) is fulfilled.
Checking if the operator fulfills (1) in eq. 40 on the boundary conditions, by checking if

$$\langle \mathcal{L}[u], v\rangle - \langle u, \mathcal{L}[v]\rangle = 0. \tag{117}$$

Ones again the boundary conditions are applied to the functions u, v.

$$\begin{aligned}
&\text{at } \gamma = 0 : b(0) = 0 \\
&\Rightarrow \qquad u(0) = 0, v(0) = 0 \\
&\text{at } \gamma = 1 : b'(1) + \widehat{Pe_a}(1)b(1) = 0 \\
&\Rightarrow \qquad u'(1) + \widehat{Pe_a}(1)u(1) = 0 \\
&\qquad\qquad\quad v'(1) + \widehat{Pe_a}(1)v(1) = 0
\end{aligned} \tag{118}$$

$$\langle \mathcal{L}_\epsilon[u], v\rangle - \langle u, \mathcal{L}_\epsilon[v]\rangle \tag{119}$$

$$= \int_0^1 \mathcal{L}_\epsilon[u]v - u\mathcal{L}_\epsilon[v]d\gamma \tag{120}$$

$$= \int_0^1 ((\mu u')' + qu)v - u((\mu v')' + qv)d\gamma \tag{121}$$

$$= \int_0^1 ((\mu u')'v - (\mu v')'ud\gamma \tag{122}$$

$$\text{using integration by parts} \tag{123}$$

$$= [\mu u'v]_0^1 - \int_0^1 \mu u'v'd\gamma - [\mu uv']_0^1 + \int_0^1 \mu u'v'd\gamma \tag{124}$$

$$= [\mu(u'v - uv')]_0^1 \tag{125}$$

$$= \mu(-\widehat{Pe_a}(1)u(1)v(1) - u(1)(-\widehat{Pe_a}(1)v(1)) \tag{126}$$

$$= -\mu\widehat{Pe_a}(1)u(1)v(1) + \mu u(1)\widehat{Pe_a}(1)v(1) \tag{127}$$

$$= 0 \tag{128}$$

Thus the operator is self-adjoint and Sturm-Liouville theory guarantees a unique solution well-defined for both boundary conditions, since the homogeneous solution will still only be the trivial.
Thus the solutions will be much more robust numerically, eigenvalues will be guaranteed real, countable, ordered and have a minimal value. It is also known that the eigenfunctions will be able to fully describe the stability of the system. No transients will begin to grow uninhibited and the solution will be non-negative always.
The problem with a non-self-adjoint operator will however, possibly give negative concentrations if only very small changes are made to a parameter. It is thus much harder to predict its behavior with different parameter values.

7.3 Case 3: Perturbation of the boundary condition

The operator does not change when case 3 is explored. $u(0) = \delta$ and $v(0) = \delta$ will not change the arguments and it follows that the operator is not self adjoint. Uniqueness is not guaranteed, and eigenvalues could be complex.

8 Numerical simulation experiment

To get an impression of how the magnitude of the advection affects the b-particles concentration profile, numerical experiments were carried out. The coefficients of the polynomial in equation 17, describing the advection, were scaled by a factor m to see the behavior of the profile. In Figure 19 five simulations are plotted alongside the steady state of a. Simulations have been done scaling $\widehat{Pe_a}(\gamma)$ with multiplication factors, $m \in [1, 5, 10, 30, 100]$. Clearly, the profile is affected by a larger advection.

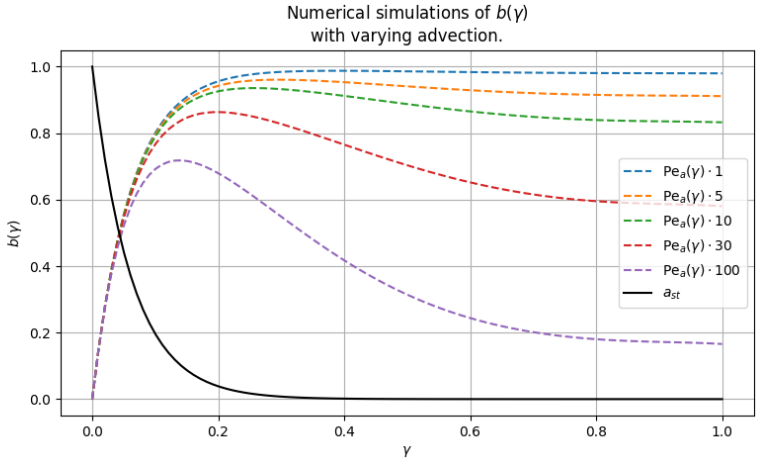

Figure 19: *Numerical experiments with scaled advection,* $\widehat{Pe_a}(\gamma)$*. Scaling factors are* $m \in [1, 5, 10, 30, 100]$. Plotting a in steady state and b in steady state for each scaling.

With scaling factor $m = 1$, the layers are not seen in the distribution of microplastics. This implies the system, with current parameter values, is dominated by diffusion instead of advection as wanted. Increasing the magnitude of the advection shows the increase in concentration as the reaction occurs and then drops again as the layer transitions.
The decrease in concentration due to $\widehat{Pe_a}(\gamma)$ dropping in magnitude, is not seen right at the transition of layers but rather an overall decrease of the concentration on the entire domain.
If we now examine the concentration at the boundary $\gamma = 1$ as a function of the scaling factor in m it is clear that the more advective driven the system becomes the less concentration occurs at $\gamma = 1$. In Figure 20 we see that the concentration decays to zero as advection is increased. This happens because of the no-flux robin boundary. The higher the concentration at $\gamma = 1$ the lower must the derivative be at the same point. This forces the solution to inflect earlier on, so the relation needed between $b(1)$ and $b'(1)$ is held at the second boundary.
This, somewhat conceptually counterintuitive phenomena, is also replicated by the implicit solution, in equation 67. In Figure 21 the same decay in concentration, when

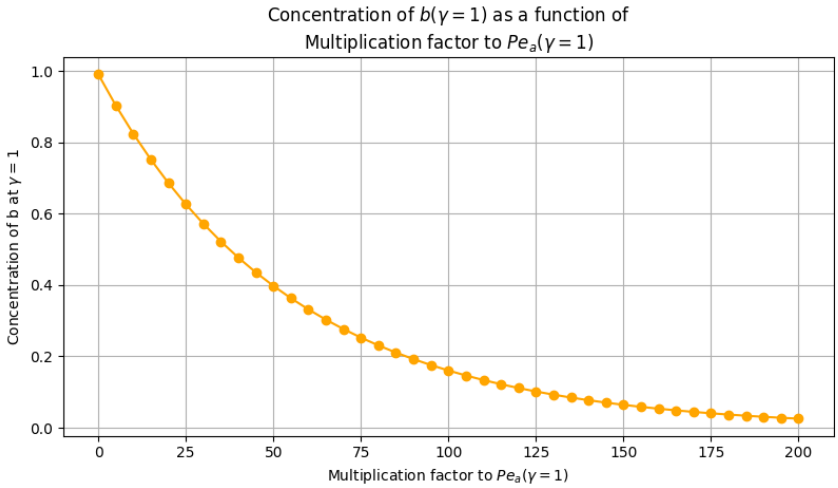

Figure 20: *Numerical simulation showing a decrease in concentration of b at the boundary* $\gamma = 1$ *as the scaling magnitude of advection increases.*

utilizing the implicit solution appears when simulated (20).

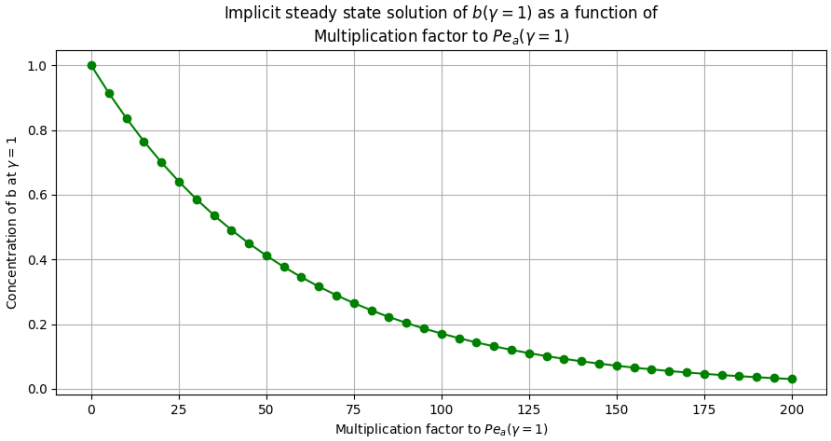

Figure 21: *Implicit solution showing a decrease in concentration of b at the boundary* $\gamma = 1$ *as the scaling magnitude of advection increases.*

9 Discussion

Solving the seemingly simple problem has showed itself to be rather cumbersome than first expected. The solution to the non-dimensionalized concentration of a, decoupled from b, converges rather quickly to its steady state. From this, an assumption that the transients in this process can be dismissed, when solving for b. As a consequence of this the solution to b will be incorrect until a has converged sufficiently.

The partial differential equations describing the overall dynamics of the system unfold on a long time scale, since by assumption no fluid flow assist in driving the transport of plastics. Therefore analyzing the analyzing the model effectively has become a task of solving ordinary differential equations. This is only feasible when boundary conditions do not vary in time. An obvious extension to the model is to include a varying boundary condition on the sea surface, since yearly maintenance of the offshore windmill park is the largest emitter of MP's. The build up in the time after such a pulse emission of MPs is an interesting effect to further investigate, since it relates closely to the real world problem. In that case the solutions can not be assumed invariant in time, and the full system of PDE's must be solved.

The spatially varying coefficient in b, $Pe_a(\gamma)$, is a polynomial, which is always continuous, analytical and well defined. Because of this an analytical solution could be found by integrating factor and it showed to match numerical simulations well. However it was found in an implicit form including several integrals. The explicit form was found but the length and form of it made it hard to interpret. Therefore power series solutions were employed.

When assuming a power series solution to the problem, the coefficients showed some special properties. For boundary conditions to be held, two degrees of freedom is needed. These are required to tune the series solution to fit both boundary conditions. The importance of having this free parameter became apparent when the solution were assumed to depend linearly on a_1 by dividing the solution into a homogenous part, c_n, and a inhomogeneous, d_n. Forcing the homogeneous part of the coefficient to be zero, since the only solution is the trivial solution turned out to give two scenarios that adhered to the coefficients a_n. Only, by allowing d_1 (Case 1.2) to be a free parameter permitted the solution to obey both boundary conditions, but did not match numerical simulations or the solution from the implicit expression.

Case 1.1 however, has $d_0 = d_1 = 0$ effectively making all coefficients equal to zero, leaving only the reaction term. It turns out that b moves as the integral of $a_{st}\theta$ over the domain $[0, \gamma]$. Calculations show that the $b(1) = -11.50$ (Figure 10) which exactly is the

$$-\int_0^1 \theta a_{st}(\gamma) d\gamma = -11.50. \tag{129}$$

In later cases where free parameters are tuned to fit the second boundary condition in different ways, we see in case 3 that $\delta = 11.50$ and in case 4 $a_1 = 11.50$. So clearly this value is a determining counterbalance of the forcing term. In case 1.2 and case 2, d_1 is tuned to have the value 11.37, however the plot does not match up with numerics. As an experiment, $d_1 = 11.50$ was carried out, and the solution matches with numerical simulations, as can be seen in the appendix Figure 28. Possible causes likely are incorrect tuning of parameters.

In case 2, perturbation of diffusion seemed to have some function in changing the qualitative solutions to the problem, since special properties are inherited by the operator, once proven it is self adjoint. However, case 2 as well did not match up with the analytical solution and numerical simulation. The free parameter d_1 did not change and the solution did not change much from the previous case. Ones, again experimentally changing $d_1 = 11.50$ changes this outcome resulting in a match to the simulation, with $\epsilon = 10^{-10}$. By letting $\epsilon \to 0$ the solution approaches the simulations.

As for case 3 a perturbation in the boundary condition allowed for non-trivial homogeneous solutions, and made a_1 become a free parameter. The second boundary condition was able to be upheld by solving the robin-boundary condition to $a_1 = 11.50$.

Case 4, is the only examined case where the solution obey both boundary conditions. The power series solution for case 4 analytical and numerical solution. This allowed a few terms of the homogeneous solution to take on values, and even though they are very small in magnitude, they let a_1 be a free parameter whilst not breaking the Dirichlet boundary condition.

The only differentiation between the water column and the sediment is by a position having the advection coefficient depend on position. This relies on the assumption that the down-flow of MPs is dominated by advective forces. In [32] pollution of solutes is modeled using a domain which has been partitioned into a water compartment and a sediment compartment, which makes it straightforward to analyze, form steady state solutions and generally to handle. But, does not make for a continuous transition between water and sediment. In truth the transition from water to sediment is not compartmentalized, environmental factors change continuously throughout the water column. Suspended material close to the seabed creates a mix of sediment and water. The closer to the seafloor the higher the amount of suspended sediment is, and therefore higher average densities. This transitional region with suspended sediment is called the Nepheloid layer. The Nepheloid layer is much more prominent at deeper seas [21]. This layer is quite under-investigated in relation to the sedimentation of microplastics.
An obvious extension of the model is include diffusive transport properties of b spatially dependent as well. With diffusion dependent on position the relationship between parameters will make for a change in the operator, and possibly give a better posed problem. This, though, is a task for further rework and analysis of the model.

The fact that only advection is dependent on position is based on an assumption that the sedimentation is dominated by advective forces. However the properties of the two layers are not seen in any of the b simulations or steady state solutions, and that the model should include other dynamics. For this reason an experiment was carried out increasing the position dependent Pechlét function $\widehat{Pe_a}(\gamma)$ to explore if the magnitude of the Pechlét function was at play. Investigation show that larger values for the Pechlét number at $\gamma = 1$ the decreases the concentration of b. This might seem conceptually counterintuitive, as higher forces are dragging the particles down, however this is caused by the no-flux boundary condition.

Only the non-dimensionalized model has been examined. Simulated concentrations will therefore only provide relative knowledge about how concentrations of MPs A and B move through the domain (with dimension). Another obvious extension to this project is to include concrete amounts of MPs emitted from windmills, perhaps with employing varying boundary conditions at $\gamma = 0$. This will certainly not be well represented by steady state solutions only, because the time dependency is relevant for future distributions of microplastics with such a dynamic.

If results are used to say something more specific, the solution can be put back into dimensional form. This has not been done in this project, since the lack of experimental data provides a poor reasoning of chosen parameter values. Therefore converting relative measures into quantities is meaningless. Future work should entail this. Data will provide a basis to form functional expressions for initial as well as boundary conditions.

A future expansion of the model could include natural decomposition. Decomposition of plastics, of the type polyurethane, occur on timescales of at least 300 years [34]. The dimensional timescale is long enough for this to be relevant, since $1\tau \approx 882$ days, which is only applicable for the chosen L and D_a. The characteristic time T grows quadratically with domain length, which in turn means that the τ could be a significantly compressed depending on the length of the domain. This gives doubt to the assumption that a steady state can be examined and be meaningful for the distribution of microplastics on a longer time scale. If decay terms were added, the reaction part would be varying in time and contribute to a time-dependent solution.

The boundary conditions chosen for the model was based on an assumption of unity concentration at $\gamma = 0$ (the sea surface) and zero-flux at $\gamma = 1$. However, the "end" of the domain is characterized by a characteristic length chosen as $L = 21$m. This is based on the depth of the sea at Horn's Rev where the modeling case originated from. However the far-field approximation of zero flux, may not be applicable on a short domain, further research into when an impermeable sediment layers begin. This can be the reason a build up forms so quickly, diffusive and advective forces drives MPs downwards, and cannot penetrate the end of the domain, but only escape through the Dirichlet boundary.

10 Conclusion

Reaction-advection-diffusion models can predict microplastic distribution in seawater and sediment, but result are sensitive to the choice of boundary conditions and functional expressions of diffusion, advection and reaction. Having only advection as a function of position, for the posed model in this project, led to incompatibilities with boundary conditions in series representations. Achieving power series solutions that are compatible with implicit solutions and numerical simulations, requires free parameters that allows for flexibility. Numerical tests show that stronger advection lowers the concentration of microplastic at the system boundary, $\gamma = 1$, which reflects the choice of boundary condition. As the model has not yet been validated with data, its predictive performance remains to be demonstrated.

11 Appendix

The appendix includes solutions to the governing equations (eqs. 24 and 25) with constant transport coefficients.

11.1 b in steady state, constant coefficients

Now examining the steady state of b. Equation 55 will be substituted into the expression of b and equated with 0. For the rest of this derivation let $\hat{d_b} = 1$ then b in steady state is as follows

$$\begin{aligned} 0 &= \tfrac{d}{\partial\gamma}\left(\tfrac{\partial b}{\partial\gamma} + \tilde{Pe_a} b\right) + \theta a_{st}(\gamma) \\ \Rightarrow \quad -\theta a_{st}(\gamma) &= \tfrac{\partial}{\partial\gamma}\left(\tfrac{\partial b}{\partial\gamma} + \tilde{Pe_a} b\right) \end{aligned} \tag{130}$$

Notice that in steady state it is purely the change in flux over position on the right side and the negated advection on the left. Defining flux:

$$\frac{\partial J}{\partial \gamma} = \theta a \tag{131}$$

Since the boundary condition imposed for a is $a(\tau, 1) = 0$ it will result in a zero flux boundary for b. The same boundary conditions are valid for the steady state in a, a_{st}. Solving for b:

$$\begin{aligned} 0 &= \frac{\partial}{\partial\gamma}\left(\frac{\partial b}{\partial\gamma} + \tilde{Pe_a} b\right) + \theta a_{st}(\gamma) \\ \Rightarrow & b''(\gamma) + \tilde{Pe_a} b'(\gamma) = -\frac{\theta}{\tilde{D}} a_{st}(\gamma) \end{aligned} \tag{132}$$

The above can be solved by dividing the solution of b in steady state, denoted b_{st}, into a homogeneous part b_h and a particular part b_p:

$$b_{st}(\gamma) = b_h(\gamma) + b_p(\gamma)$$

The homogeneous part is found by setting:

$$0 = \frac{\partial}{\partial\gamma}\left(\frac{\partial b}{\partial\gamma} + \tilde{Pe_a} b\right) \tag{133}$$

solving by finding the eigenvalues $\lambda_1 = -\xi$ and $\lambda_2 = 0$ and inserting in the general solution yields

$$b_h(\gamma) = C_1 e^{-\tilde{Pe_a}\gamma} + C_2. \tag{134}$$

The particular part is found by the method of undetermined coefficients. Since the reaction term of the equation is made up of hyperbolic sine functions, which can be rewritten using the relation $sinh(x) = (e^x - e^{-x})/2$, and therefore a natural guess of the particular solution is

$$b_p(\gamma) = C_3 e^{-\sqrt{\theta}\gamma} + C_4 e^{\sqrt{\theta}\gamma} \tag{135}$$

Computing the first and second derivative of eq. 135 and inserting into equation 132 yields

$$C_3\theta e^{-\sqrt{\theta}\gamma} + C_4\theta e^{\sqrt{\theta}\gamma} + \tilde{Pe}_a(-C_3\sqrt{\theta}e^{-\sqrt{\theta}\gamma} + C_4\sqrt{\theta}e^{\sqrt{\theta}\gamma}) + \theta a_{st}(\gamma) = 0. \tag{136}$$

$a_{st}(\gamma)$ can also be expanded as

$$a_{st}(\gamma) = \frac{1}{2\sinh(\sqrt{\theta})}(e^{\sqrt{\theta}}e^{-\sqrt{\theta}\gamma} - e^{-\sqrt{\theta}}e^{\sqrt{\theta}\gamma}).$$

Since the relation in 136 must be true for every γ, the coefficients related to $e^{\sqrt{\theta}\gamma}$ and $e^{-\sqrt{\theta}\gamma}$ must be equal to zero. Therefore the following relations hold; first the coefficient related to $e^{-\sqrt{\theta}\gamma}$

$$C_3\theta - \tilde{Pe}_a C_3\sqrt{\theta} = -\frac{\theta e^{\sqrt{\theta}}}{2\sinh\sqrt{\theta}}. \tag{137}$$

And the coefficient for $e^{\sqrt{\theta}\gamma}$

$$C_4\theta + \tilde{Pe}_a C_4\sqrt{\theta} = \frac{\theta e^{-\sqrt{\theta}}}{2\sinh\sqrt{\theta}}. \tag{138}$$

Isolating and solving for C_3 and C_4 yields

$$\begin{aligned} C_3 &= -\frac{\theta e^{\sqrt{\theta}}/2\sinh(\sqrt{\theta})}{\theta - \tilde{Pe}_a\sqrt{\theta}}, \\ C_4 &= \frac{\theta e^{\sqrt{-\theta}}/2\sinh(\sqrt{\theta})}{\theta + \tilde{Pe}_a\sqrt{\theta}}. \end{aligned} \tag{139}$$

This gives the general solution:

$$b(\gamma) = -\frac{\theta e^{\sqrt{\theta}}/2\sinh(\sqrt{\theta})}{\theta - \tilde{Pe}_a\sqrt{\theta}}e^{-\sqrt{\theta}\gamma} + \frac{\theta e^{\sqrt{-\theta}}/2\sinh(\sqrt{\theta})}{\theta + \tilde{Pe}_a\sqrt{\theta}}e^{\sqrt{\theta}\gamma} + C_1e^{-\xi\gamma} + C_2 \tag{140}$$

Inferring the boundary conditions and inserting parameter values give:

$$\begin{aligned} C_2 &= 0 \\ C_1 &= 1.25 \end{aligned}$$

And the final specific solution is

$$b(\gamma) = -\frac{\theta e^{\sqrt{\theta}}/2\sinh(\sqrt{\theta})}{\theta - \tilde{Pe}_a\sqrt{\theta}}e^{-\sqrt{\theta}\gamma} + \frac{\theta e^{\sqrt{-\theta}}/2\sinh(\sqrt{\theta})}{\theta + \tilde{Pe}_a\sqrt{\theta}}e^{\sqrt{\theta}\gamma} + 1.25e^{-\xi\gamma} \tag{141}$$

In figure 22 the steady state solution (eq. 141) is plotted.
Numerical simulations show that the solution to converge numerically to the found steady state solution.

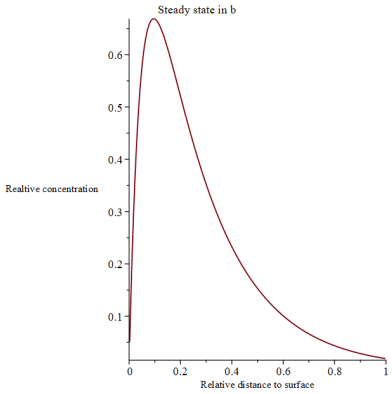

Figure 22: *b in steady state with constant transport coefficients, and chosen parameter values*

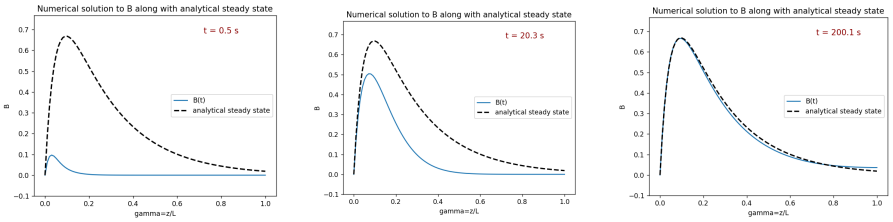

(a) Numerical solution at t=0.5 s (b) Numerical solution at t=20.3 s (c) Numerical solution at t=200.3 s

Figure 23: *Convergence of numerical solution to steady state solution of b*

11.2 Full analytical solution of a

For the remainder of the solving the analytical solution of a let $k = -\alpha$.
Because of the exponential in initial and boundary conditions, this seemingly simple system cannot be solved. This because separation of variables homogeneous boundary conditions. Another method is thus used to solve the system, where we assume that the system will reach a steady state as $t \to \infty$. Thus the system solution is written up as a steady state solution a_{st} and an "influence" upon the steady state v as such: [Hansen]

$$v(\gamma, \tau) = a(\gamma, \tau) - a_{st}(\gamma) \tag{142}$$

From earlier we have a full expression of the steady state problem:

$$a_{st}(\gamma) = \frac{sinh(\sqrt{\theta}(1-\gamma))}{sinh(\sqrt{\theta})} \tag{143}$$

Now rewriting the boundary conditions:

$$v(0,\tau) = v(1,\tau) = 0 \tag{144}$$

and the initial condition:

$$v(\gamma,0) = a(\gamma,0) - a_{st}(\gamma) = \frac{e^{-g\gamma} - e^{-g}}{1 - e^{-g}} - a_{st}(\gamma) \tag{145}$$

This is a problem known to have Fourier sine series as a solution [Hansen], on the form:

$$v(\gamma,\tau) = \sum_{n=1}^{\infty} b_n sin(n\pi\gamma)d\gamma \tag{146}$$

with coefficients:

$$b_n = 2\int_0^L v(0,\gamma)sin(n\pi\gamma)d\gamma \tag{147}$$

a solution is found by inserting into eq. 142:

$$a(\gamma,\tau) = a_{st}(\gamma) + \sum_{n=1}^{\infty} b_n sin(n\pi\gamma)e^{-((n\pi)^2+\theta)\tau}d\gamma \tag{148}$$

with the given coefficients calculated using maple.

11.2.1 Results

In Figure 24 the difference between the initial condition of the system and the steady state can be seen. It is seen that the system only evolves very little between the two stages. In Figure 24, 50 terms of equation 148 with $\theta = 441$ is plotted. 50 terms of the sum has been included and the coefficient seems to converge (figure 25)
In Figure 26 the development over 10 time-steps can be seen. Not surprisingly, based on Figure 24, it does not evolve much in time and approaches the steady state solution. From numerical solutions we get an impression of how fast the solution converges to its steady state from the initial condition. Here the average error is given by the mean of the absolute difference between the curves at each point.
It is seen to steadily converge toward the steady state and is very quickly only deviating from it with an order of 10^{-4}.

11.3 Case 1.2

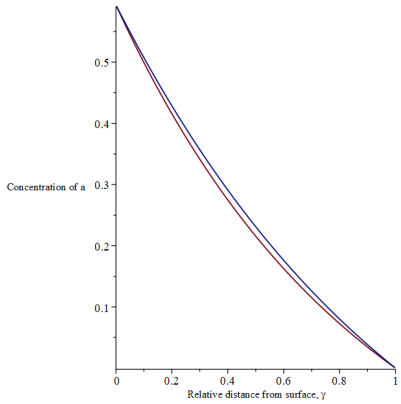

Figure 24: *Analytical steady state solution plotted along with the initial condition a (eq.* 148).

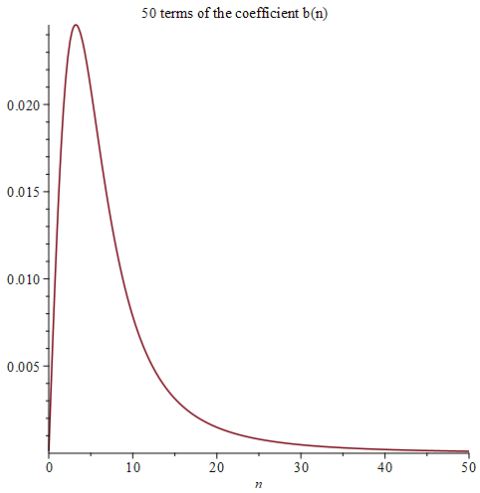

Figure 25: *50 terms of the coefficient in full solution of a (equation)*

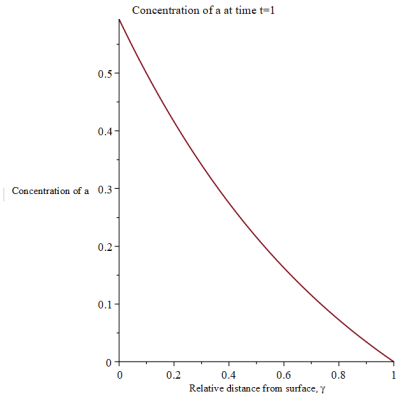

(a) Analytical solution to time t=1

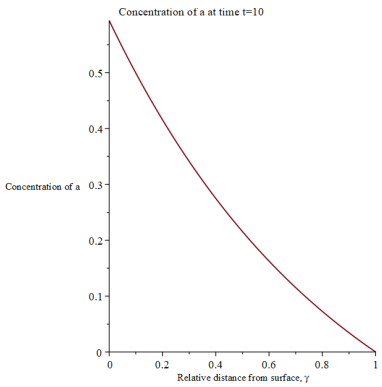

(b) Analytical solution to time t=10

Figure 26: *Concentration of a at two time points, t=1 and t=10. Illustrating the development over time.*

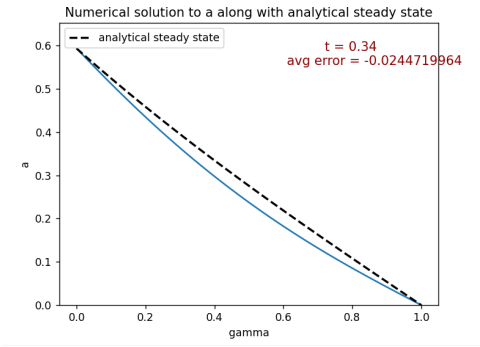

(a) *Numeric solution to a at time τ=0.34*

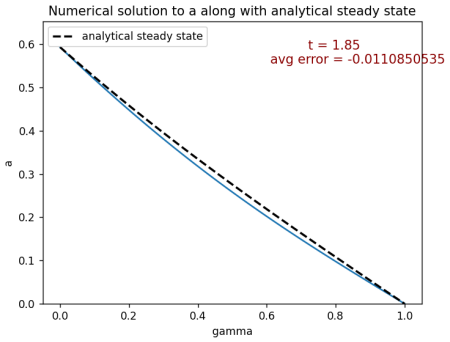

(b) *Numeric solution to a at time τ=1.85*

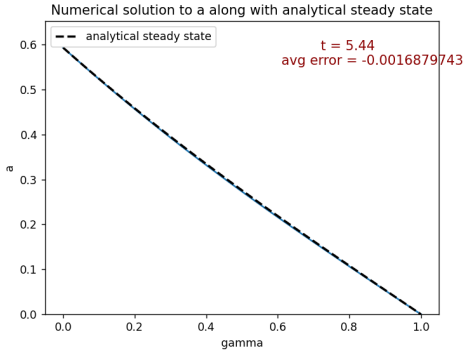

(c) *Numeric solution to a at time τ=5.44*

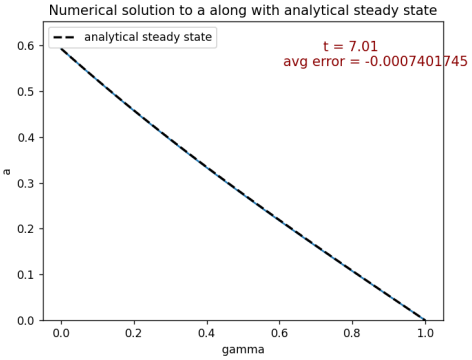

(d) *Numeric solution to a at time τ=7.01*

Figure 27: *Numerical solution to $a(\gamma, \tau)$*

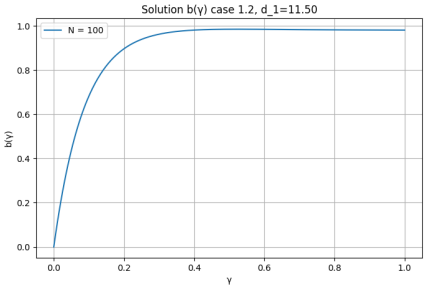

Figure 28: Case 1.2 with adjusted $d_1 = 11.50$

12 Bibliography

[1] Al-Zawaidah, H., Kooi, M., Hoitink, T., Vermeulen, B., & Waldschlager, K. (2024). Mapping microplastic movement: A phase diagram to predict nonbuoyant microplastic modes of transport at the particle scale. *Environmental Science & Technology*, 58(40), 17979–17989.

[2] Amaral-Zettler, L. A., Zettler, E. R., Mincer, T. J., Klaassen, M. A., & Gallager, S. M. (2021). Biofouling impacts on polyethylene density and sinking in coastal waters: a macro/micro tipping point? *Water Research*, 201, 117289.

[3] Christensen, O. (2012). *Differentialligninger og uendelige rækker*. Technical University of Denmark.

[Claudia Lorenz] Claudia Lorenz. Meetings and email correspondance with Claudia.

[5] Daewel, U., Akhtar, N., Christiansen, N., & Schrum, C. (2022). Offshore wind farms are projected to impact primary production and bottom water deoxygenation in the north sea. *Communications Earth & Environment*, 3(1), 292.

[6] Dichgans, F., Boos, J.-P., Ahmadi, P., Frei, S., & Fleckenstein, J. H. (2023). Integrated numerical modeling to quantify transport and fate of microplastics in the hyporheic zone. *Water Research*, 243, 120349.

[7] Dimante-Deimantovica, I., Saarni, S., Barone, M., Buhhalko, N., Stivrins, N., Suhareva, N., Tylmann, W., Vianello, A., & Vollertsen, J. (2024). Downward migrating microplastics in lake sediments are a tricky indicator for the onset of the anthropocene. *Science advances*, 10(8), eadi8136.

[8] Energistyrelsen (2025). Etablerede havvindmølleparker. Accessed: 2025-11-20.

[Environmental litteracy council] Environmental litteracy council. How much plastic is in the ocean 2023?

[10] et al, M. L. A. K. (2023). Global mass of buoyant marine plastics dominated by large long-lived debris. *Nature Geoscience*.

[11] FAO (2021). Assessment of agricultural plastics and their sustainability. a call for action. *FAO rome*.

[12] Galey, P. (2019). Clues emerge in 'missing' ocean plastics conundrum. *phys.org*.

[13] Galgani, F., Hanke, G., & Maes, T. (2015). Global distribution, composition and abundance of marine litter. In *Marine anthropogenic litter* (pp. 29–56). Springer International Publishing Cham.

[14] Gunalaan, K., L. C. A. R. e. a. (2023). Does water column stratefication influence the vertical distribution of microplastics? *Environmental pollution*.

[Hansen] Hansen, J. S. A note on the reaction-diffusion equation. Fall 2024.

[16] Herman, R. L. (2005). *A secondary course in ordinary differential equations: dynamical systems and boundary value problems*. University of North Carolina Wilmington.

[17] Jolaosho, T. L., Rasaq, M. F., Omotoye, E. V., Araomo, O. V., Adekoya, O. S., Abolaji, O. Y., & Hungbo, J. J. (2025). Microplastics in freshwater and marine ecosystems: Occurrence, characterization, sources, distribution dynamics, fate, transport processes, potential mitigation strategies, and policy interventions. *Ecotoxicology and Environmental Safety*, 294, 118036.

[18] Kim, J., Poirier, D. G., Helm, P. A., Bayoumi, M., & Rochman, C. M. (2020). No evidence of spherical microplastics (10–300 μm) translocation in adult rainbow trout (oncorhynchus mykiss) after a two-week dietary exposure. *PLoS One*, 15(9), e0239128.

[19] King, R. P. (2002). *Introduction to practical fluid flow*. Elsevier.

[20] Kristensen, E., Penha-Lopes, G., Delefosse, M., Valdemarsen, T., Quintana, C. O., & Banta, G. T. (2012). What is bioturbation? the need for a precise definition for fauna in aquatic sciences. *Marine ecology progress series*, 446, 285–302.

[21] McCave, I. (2019). Nepheloid layers. In J. K. Cochran, H. J. Bokuniewicz, & P. L. Yager (Eds.), *Encyclopedia of Ocean Sciences (Third Edition)* (pp. 170–183). Oxford: Academic Press, third edition edition.

[22] Mendrik, F., Fernández, R., Hackney, C. R., Waller, C., & Parsons, D. R. (2023). Non-buoyant microplastic settling velocity varies with biofilm growth and ambient water salinity. *Communications Earth & Environment*, 4(1), 30.

[Microplastics] Microplastics. Everything you should know about microplastics. UN environment program.

[24] OECD (2024). Policy scenarios for eliminating plastic pollution by 2040. *OECD*.

[25] Pedersen, J., Leonhard, S. B., Klaustrup, M., & Hvidt, C. B. (2006). Benthic communities at horns rev before, during and after con-struction of horns rev offshore wind farm.

[26] Qin, Y., Tu, Y., Chen, C., Wang, F., Yang, Y., & Hu, Y. (2024). Biofilms on microplastic surfaces and their effect on pollutant adsorption in the aquatic environment. *Journal of Material Cycles and Waste Management*, 26(6), 3303–3323.

[27] Recktenwald, G. (2014). Ftcs solution to the heat equation. *Course ME*, 448, 548.

[28] Røed, L. P. (2018). Advection problem. In *Atmospheres and Oceans on Computers: Fundamental Numerical Methods for Geophysical Fluid Dynamics* (pp. 75–114). Springer.

[29] Ryan, P. G. (2015). A brief history of marine litter research. In *Marine anthropogenic litter* (pp. 1–25). Springer International Publishing Cham.

[30] Saba, G. K. & Steinberg, D. K. (2012). Abundance, composition and sinking rates of fish fecal pellets in the santa barbara channel. *Scientific Reports*, 2(1), 716.

[31] Strauss, W. A. (2008). *Partial Differential Equations, second edition.* John Wiley and sons, Ltd.

[32] Timmermann, K., Christensen, J. H., & Banta, G. T. (2002). Modeling of advective solute transport in sandy sediments inhabited by the lugworm arenicola marina. *Journal of Marine Research.*

[33] Tom M. Nolte a b, Nanna B. Hartmann a, J. M. K. c. J. G. d. D. v. d. M. b. e. A. J. H. b. A. B. a. (2017). The toxicity of plastic nanoparticles to green algae as influenced by surface modification, medium hardness and cellular adsorption. *Aquatic Toxicology.*

[34] X. Zhang, C. X. P. (2022). How long for plastics to decompose in the deep sea? *Geochemical Perspectives Letters v22.*

[35] Xia Zhu a, Chelsea M. Rochman b, B. D. H. c. C. W. d. (2024). Plastics in the deep sea – a global estimate of the ocean floor reservoir. *Deep Sea Research Part I: Oceanographic Research Papers.*